



3 4456 0360966 4

ORNL-1289
Progress

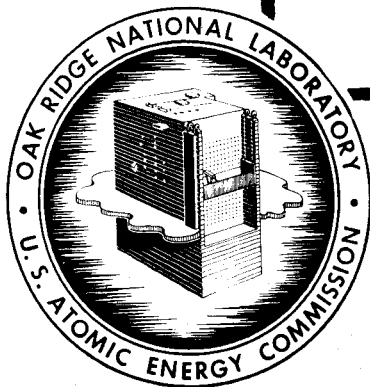
~~8A~~

8A

PHYSICS DIVISION

QUARTERLY PROGRESS REPORT

FOR PERIOD ENDING MARCH 20, 1952



LIBRARY

DO NOT TRANSFER TO OTHER DIVISION

If you wish someone to borrow this report, send in name with department and the Library will arrange a loan.

OAK RIDGE NATIONAL LABORATORY
OPERATED BY
CARBIDE AND CARBON CHEMICALS COMPANY
A DIVISION OF UNION CARBIDE AND CARBON CORPORATION



POST OFFICE BOX P
OAK RIDGE, TENNESSEE

ORNL-1289

This document consists of 54 pages.

Copy 8 of 330 copies. Series A.

Contract No. W-7405-eng-26

PHYSICS DIVISION
QUARTERLY PROGRESS REPORT
for Period Ending March 20, 1952

A. H. Snell, Director
E. O. Wollan, Associate Director

DATE ISSUED

OAK RIDGE NATIONAL LABORATORY
operated by
CARBIDE AND CARBON CHEMICALS COMPANY
A Division of Union Carbide and Carbon Corporation
Post Office Box P
Oak Ridge, Tennessee



3 4456 0360966 4



INTERNAL DISTRIBUTION

- | | | | |
|--------|---|--------|----------------------|
| 1. | G. T. Felbeck (C&CCC) | 34. | L. D. Roberts |
| 2-3. | Chemistry Library | 35. | J. A. Lane |
| 4. | Physics Library | 36. | R. N. Lyon |
| 5. | Biology Library | 37. | W. C. Koehler |
| 6. | Health Physics Library | 38. | W. K. Ergen |
| 7. | Metallurgy Library | 39. | E. P. Blizard |
| 8-9. | Training School Library | 40. | M. E. Rose |
| 10. | Reactor Experimental
Engineering Library | 41. | G. E. Boyd |
| 11-14. | Central Files | 42. | Lewis Nelson |
| 15. | C. E. Center | 43. | R. W. Stoughton |
| 16. | C. E. Larson | 44. | C. E. Winters |
| 17. | W. B. Humes (K-25) | 45. | W. H. Jordan |
| 18. | L. B. Emlet (Y-12) | 46. | E. C. Campbell |
| 19. | A. M. Weinberg | 47. | D. S. Billington |
| 20. | E. H. Taylor | 48. | M. A. Bredig |
| 21. | E. D. Shipley | 49. | R. S. Livingston |
| 22. | E. J. Murphy | 50. | C. P. Keim |
| 23. | F. C. VonderLage | 51. | J. L. Meem |
| 24. | A. H. Snell | 52. | C. E. Clifford |
| 25. | J. A. Swartout | 53. | G. H. Clewett |
| 26. | A. Hollaender | 54. | C. D. Susano |
| 27. | K. Z. Morgan | 55. | C. J. Borkowski |
| 28. | F. L. Steahly | 56. | M. J. Skinner |
| 29. | M. T. Kelley | 57. | L. A. Rayburn |
| 30. | E. M. King | 58. | S. Bernstein |
| 31. | E. O. Wollan | 59. | P. M. Reyling |
| 32. | D. W. Cardwell | 60. | D. D. Cowen |
| 33. | A. S. Householder | 61-75. | Central Files (O.P.) |

EXTERNAL DISTRIBUTION

- 76-330. Given distribution as shown in TID 4500 under Physics Category.

Physics Division quarterly progress reports previously issued in this series are as follows:

ORNL-325 Supplement	December, January, and February, 1948-1949
ORNL-366	Period Ending June 15, 1949
ORNL-481	Period Ending September 25, 1949
ORNL-577	Period Ending December 15, 1949
ORNL-694	Period Ending March 15, 1950
ORNL-782	Period Ending June 15, 1950
ORNL-865	Period Ending September 20, 1950
ORNL-940	Period Ending December 20, 1950
ORNL-1005	Period Ending March 20, 1951
ORNL-1092	Period Ending June 20, 1951
ORNL-1164	Period Ending September 20, 1951
ORNL-1278	Period Ending December 20, 1951

TABLE OF CONTENTS

	PAGE
SUMMARY	1
1. HIGH-VOLTAGE PHYSICS	3
Energy Spectrum of Protons from He ³ Bombarded by He ³	3
Energy Spectrum of Particles from H ³ Bombarded by He ³	3
Gamma Rays from Proton Bombardment of Light Elements	5
Inelastic Scattering	7
The H ³ (p,γ)He ⁴ Reaction	7
The C ¹³ (p,n)N ¹³ Reaction	7
The B ¹¹ (p,n)C ¹¹ Angular Distribution	7
(p,n) Thresholds in Neon	9
2. RADIOACTIVITY AND NUCLEAR ISOMERISM	10
Angular Correlation of Gamma Rays	10
Gamma-Gamma Angular Correlations in Ta ¹⁸¹	10
K-Shell Internal Conversion Coefficient Measurements	11
3. NEUTRON DIFFRACTION	12
Neutron Diffraction Studies on Superconducting Elements	12
Neutron Diffraction Studies of Some Rare Earths	13
Magnetic Structure of Mn ₂ Sb	14
Total Neutron Cross Sections at Indium Resonance Energy (1.44 ev)	15
4. LOW-TEMPERATURE PHYSICS	16
Specific Heat of Neodymium Ethyl Sulfate from 1 to 2°K	16
Measurement of the Weiss Constant in Copper Potassium Sulfate	18
Superconductivity of a Hafnium-Zirconium Alloy	19
5. HEAVY-ION PHYSICS	20
Space Distribution of Ionization in a Gas	20
6. NEUTRON DECAY AND NEUTRON CROSS SECTIONS	34
Neutron Decay	34
Time-of-Flight Spectrometer	36
Pile Oscillator Measurements	36
7. THEORETICAL PHYSICS	38
Status of Current Work	38
Tabulation of the Racah Coefficients	38
Theory of the T + D Reaction	38
The Parameterization of Quantum Electrodynamics	39



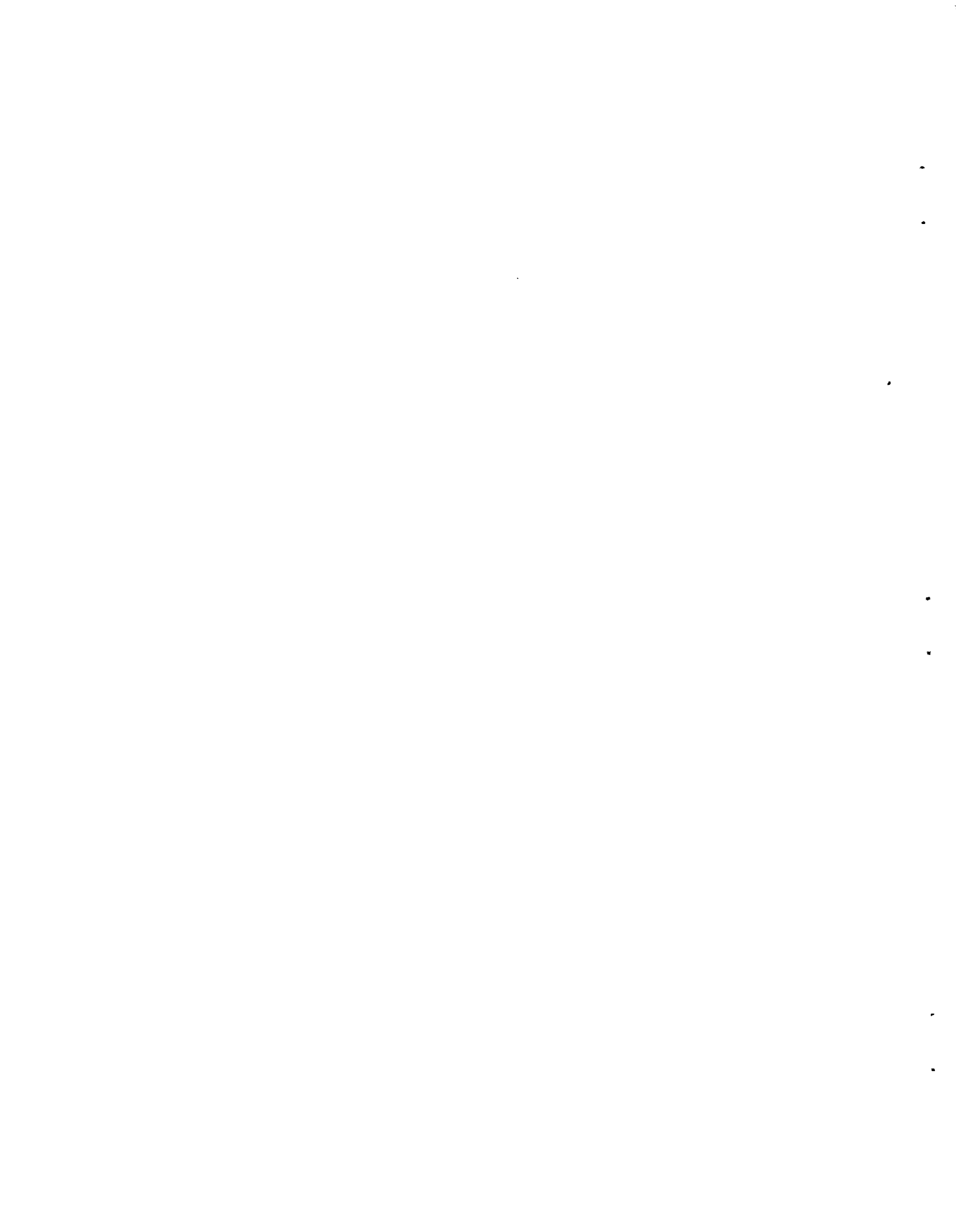
LIST OF FIGURES

FIGURE	TITLE	PAGE
1.1	Apparatus for Bombardment of He^3 by He^3	3
1.2	Energy Spectrum of Protons in the Reactions $\text{He}^3 \left[\begin{array}{c} \text{He}^3, \text{Li}^5 \\ \text{He}^4, \text{H}^1 \end{array} \right] \text{H}^1$	4
1.3	Apparatus for Bombardment of H^3 by He^3	5
1.4	Energy Spectrum of Particles Accompanying Breakup of Li^6 Formed by He^3 Capture on H^3	6
1.5	Energy Spectrum of Particles from $\text{He}^3 + \text{H}^3$ Reaction With and Without Aluminum Absorber	6
1.6	Yield of the $\text{C}^{13}(p,n)\text{N}^{13}$ Reaction in the Forward Direction	8
1.7	Yield of the $\text{B}^{11}(p,n)\text{C}^{11}$ Reaction at $\theta_{\text{lab}} = 0^\circ$	9
4.1	Magnetic Susceptibility of Copper Potassium Sulfate, $\text{CuK}_2(\text{SO}_4)_2 \cdot 6\text{H}_2\text{O}$	19
5.1	Differential Pumping System and Isoionization Chamber	21
5.2	Isoionization Density Contours for He^+ in Argon	22
5.3	Isoionization Density Contours for A^+ in Argon	23
5.4	Isoionization Density Contours for A^+ in Helium	23
5.5	Effect of Pressure on Contour Length of He^+ in Argon	24
5.6	Effect of Pressure on Contour Shape of He^+ in Argon and A^+ in Helium	25
5.7	Effect of Pressure on Contour Length of A^+ in Argon	26
5.8	Effect of Pressure on Contour Shape of A^+ in Argon	26
5.9	Effect of Pressure on Contour Length of He^+ in Helium	27
5.10	Effect of Pressure on Contour Shape of He^+ in Helium	28
5.11	Isoionization Density Contours of i/p^2 Equal to 1.0 and 0.2 for He^+ in Helium, He^+ in Argon, and A^+ in Argon, Each Converted to Atmospheric Pressure	29
5.12	Axial Ionization Chamber Current for A^+ in Argon	30
5.13	Equirange Contour for $R = 5.0$ in., A^+ in Argon	31
5.14	Integration of $ir dr$ for A^+ in Argon for $R = 5.0$ Inches	32
5.15	Computation of Range from Isoionization Data	33

FIGURE	TITLE	PAGE
5.16	Curve Fitting of the Function $i(R, r) = e^{-AR-B(r^2/R^2)}$ for A^+ in Argon	34
6.1	Transmission Measurements of Indium Isotopes with Time-of-Flight Spectrometer	37

LIST OF TABLES

TABLE	TITLE	PAGE
2.1	Experimental and Theoretical Internal Conversion Coefficients	11
3.1	Cross Sections at 1.44 ev	15
4.1	Isotopic Composition of the Neodymium Used to Prepare the Samples	16
4.2	Measurements of b/C on Three Neodymium Samples	17
4.3	Simultaneous Equations for Specific Heats of Neodymium Samples	18
6.1	Capture Cross Sections	36



PUBLICATIONS

A list of publications by members of the Physics Division is as follows:

M. E. Rose, L. C. Biedenharn, and G. B. Arfken, "Internal Conversion Angular Correlations," *Phys. Rev.* **85**, 5 (1952).

F. K. McGowan, "Lifetime of an Excited State of ${}_{66}\text{Dy}^{160}$ and Upper Limits for Some Other Nuclei," *Phys. Rev.* **85**, 142 (1952).

F. K. McGowan, "Measurements of Some K-Shell Internal Conversion Coefficients," *Phys. Rev.* **85**, 151 (1952).

F. K. McGowan, E. D. Klema, and P. R. Bell, "Classification of the γ -Radiation of Hf^{177} ," *Phys. Rev.* **85**, 152 (1952).

W. C. Koehler and E. O. Wollan, "The Coherent Neutron Scattering Cross Section of C^{13} ," *Phys. Rev.* **85**, 491 (1952).

H. B. Willard, J. K. Bair, J. D. Kington, T. M. Hahn, C. W. Snyder, and F. P. Green, "The Yield of Gamma-Rays and Neutrons from the Proton Bombardment of Fluorine," *Phys. Rev.* **85**, 849 (1952).

J. Schenck and R. L. Heath, "Tin Activation of LiI," *Phys. Rev.* **85**, 923 (1952).

C. D. Moak, W. M. Good, and W. E. Kunz, "The Reaction $\text{Li}^6(t,p)\text{Li}^8$," *Phys. Rev.* **85**, 928 (1952).

C. H. Johnson, G. P. Robinson, and C. D. Moak, "Capture Gamma-Rays from 277-Kev Protons on N^{14} ," *Phys. Rev.* **85**, 931 (1952).

T. M. Hahn, C. W. Snyder, H. B. Willard, J. K. Bair, E. D. Klema, J. D. Kington, and F. P. Green, "Neutrons and Gamma-Rays from the Proton Bombardment of Beryllium," *Phys. Rev.* **85**, 934 (1952).

J. K. Bair, H. B. Willard, C. W. Snyder, T. M. Hahn, J. D. Kington, and F. P. Green, "Proton Bombardment of Lithium," *Phys. Rev.* **85**, 946 (1952).

ANNOUNCEMENTS

J. L. Fowler, who was previously associated with the Electromagnetic Division, has been transferred to the Physics Division as leader, with W. M. Good, of the High Voltage Physics group.

W. E. Kunz and G. S. Pawlicki finished their doctoral thesis research under ORINS fellowships and are now employed by the division. Kunz is with the High Voltage group and Pawlicki is working with the time-of-flight spectrometer.

R. C. Keen, on leave from Louisiana State University, is working with the Critical Experiments group.

N. S. Gingrich, on leave from the University of Missouri, is spending six months on neutron-diffraction problems.

L. S. Abbott, who was formerly associated with the Technical Publications Department, has been transferred to the Physics Division and is now assisting with the editing of reports and in addition is associated with the Shielding group.

PHYSICS DIVISION QUARTERLY PROGRESS REPORT

SUMMARY

High-Voltage Physics. The investigation of (p,n) reactions on the 5-Mev Van de Graaff has continued. The (p,n) thresholds of Ne^{21} and Ne^{22} have been determined, and the yield of the $\text{C}^{13}(p,n)\text{N}^{13}$ reaction at zero degrees has been measured from threshold (3.24 Mev) to 5 Mev. The results indicate a number of energy levels in the compound nucleus, N^{14} . The absolute differentiation cross section of the $\text{B}^{11}(p,n)\text{C}^{11}$ reaction has been measured as a function of angle and energy.

Several preliminary investigations of the gamma rays produced by nuclear reactions have been carried out by detection with NaI crystals. Measurement of the gamma-ray yield from inelastic scattering of neutrons from boron, fluorine, aluminum, and magnesium shows discontinuities, some of which occur at energies corresponding to known levels of the nuclei concerned. The yield of 20-Mev gamma rays from the $\text{H}^3(p,\gamma)\text{He}^4$ reaction shows a general increase from 1 to 5 Mev.

Relative (p,γ) yields have been determined from bombardments of Li^6 , C^{13} , and N^{15} by protons from the 2-Mev Van de Graaff.

Energy spectra have been obtained with improved resolution of the particles resulting from the breakup of Li^6 and Be^6 formed by bombarding H^3 and He^3 , respectively, with He^3 . Results concerning the ground state of He^5 and Li^5 are discussed.

Radioactivity and Nuclear Isomerism. Measurements have been made of the angular correlation of the gamma rays from Ba^{134} and Cd^{114} , but the decay schemes for these nuclides have not

yet been definitely established. Angular correlations have also been measured for several gamma-ray cascades in Ta^{181} that follow the beta decay of Hf^{181} . The correlation of the 132-keV with the 480-keV gamma ray was found to be anisotropic, but the observed anisotropy cannot be reconciled with an $E2$ transition that is indicated by the K -shell conversion coefficients.

K -shell internal conversion coefficients have been measured for the gamma-ray transitions in La^{139} and Te^{123} .

Neutron Diffraction. Neutron diffraction studies have been made of a number of superconducting metals at temperatures above and below the transition temperatures. In no case was any electronic scattering effect observed either of a coherent or incoherent nature, and there is no noticeable change in the atomic lattice vibrations.

Coherent cross sections have been determined for Sm^{152} and Sm^{154} ; a negative scattering amplitude is observed for the lighter isotope. Measurements of the diffuse scattering by Pr_2O_3 and Nd_2O_3 have shown no measurable paramagnetic scattering for these rare-earth ions.

A preliminary analysis has been made of the magnetic structure of Mn_2Sb from neutron diffraction data.

Low-Temperature Physics. Measurements of the specific heat of neodymium ethyl sulfate have been made in the temperature region from 1 to 2°K on samples with different isotopic enrichment. The specific heat constants were obtained for the hyperfine

PHYSICS DIVISION QUARTERLY PROGRESS REPORT

splitting in Nd^{143} and Nd^{145} and for the electron-electron interaction that was found to have an unusually low value.

The superconducting transition temperature of a sample of 90 at. % Hf and 10 at. % Zr was measured and was found to agree with previous measurements on pure hafnium metal.

Heavy-Ion Physics. The spatial distribution of the ionization in various gases produced by a collimated beam of heavy ions has been measured for different types of ions over a range of initial energies. The beam is passed through a pinhole into the gas chamber, and the ionization is measured with a small ionization chamber that can be moved throughout the volume. Contour maps of equal ionization density are shown in a number of figures and the significance of the results are discussed.

Neutron Decay and Neutron Cross Sections. The emphasis in the neutron decay experiment has shifted to the study of the angular correlation between the beta particle and the proton and hence the neutrino. A discussion is given of the proposed

plan for attacking this problem and of the status of the equipment.

The neutron time-of-flight spectrometer has been applied to the study of resonances in In^{113} and In^{115} and copper; some new resonances have been observed.

Recent measurements of capture cross sections with the pile oscillator include potassium and the isotopes of calcium, iron, and barium. This brings the number of isotopes measured to more than 100.

Theoretical Physics. The status of current theoretical work including *L*-shell conversions, Fermi functions, angular correlations, and Racah coefficients is reviewed.

A theoretical extension of the work of Flowers is given for the tritium plus deuterium reaction, but the results are found to disagree with experimental data. A different method of attack on the problem is suggested.

The single-particle formulation of relativistic quantum electrodynamics is extended in several directions over the work reported in the previous quarterly.

1. HIGH-VOLTAGE PHYSICS

ENERGY SPECTRUM OF PROTONS FROM He³
BOMBARDED BY He³

W. M. Good C. D. Moak
 W. E. Kunz

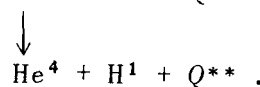
A preliminary attempt to obtain the spectrum of protons emitted following the capture of He³ by He³ was described in previous reports.⁽¹⁾ Be⁶, which is formed in the compound state of the reaction, breaks up in two modes,



amplifiers with pulse heights set so that the He³(He³,H¹,H¹)He⁴ protons in a given energy range served as a monitor. The spectrum observed by means of a differential pulse-height spectrometer was normalized to monitor counts. As in the previous experiment, the target was built up in aluminum by the He³⁺ beam; the bombarding energy was 320 kev.

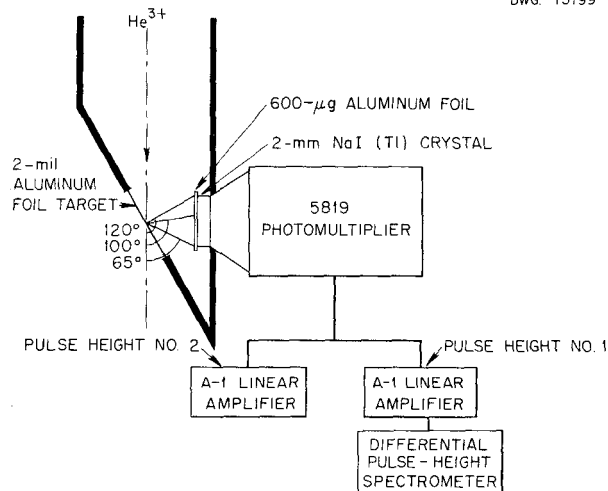
$$\text{He}^4 + \text{H}^1 + \text{H}^1 + 12.81 \text{ Mev} \quad (1)$$

$$\text{Li}^5 + \text{H}^1 + Q^* \quad (2)$$



The previous experiment failed to reveal any group structure in the spectrum corresponding to levels in Li⁵. This failure was attributed to (1) the thickness of the aluminum (1 mil) through which the protons passed before entering the spectrometer, (2) the difficulty in hitting the target, which made microcoulomb measurements meaningless, and (3) the predominance of the contaminating He³(H²,H¹)He⁴ reaction, which made it impossible to use the integral pulse counts as a monitor.

The experiment has been repeated by using the arrangement shown in Fig. 1.1. The NaI crystal for the spectrometer was mounted in the high vacuum and was shielded from the scattered He³⁺ beam by means of a 600-μg aluminum foil. The pulse from the 5819 photo-multiplier went to two A-1 linear



UNCLASSIFIED
DWG. 15199

Fig. 1.1. Apparatus for Bombardment of He³ by He³.

The spectrum obtained is shown in Fig. 1.2. The end point of the observed distribution is within 3% of the expected maximum energy. The slight maximum near the end of the distribution needs further confirmation because of the possibility of systematic error. Interpretation of the peak requires assumptions regarding the

⁽¹⁾W. M. Good, W. E. Kunz, and C. D. Moak, "The Reaction of He³ + He³," *Physics Division Quarterly Progress Report for Period Ending June 20, 1951*, ORNL-1092, p. 21; W. M. Good, W. E. Kunz, and C. D. Moak, "Charged-Particle Reactions," *Physics Division Quarterly Progress Report for Period Ending September 20, 1951*, ORNL-1164, p. 30.

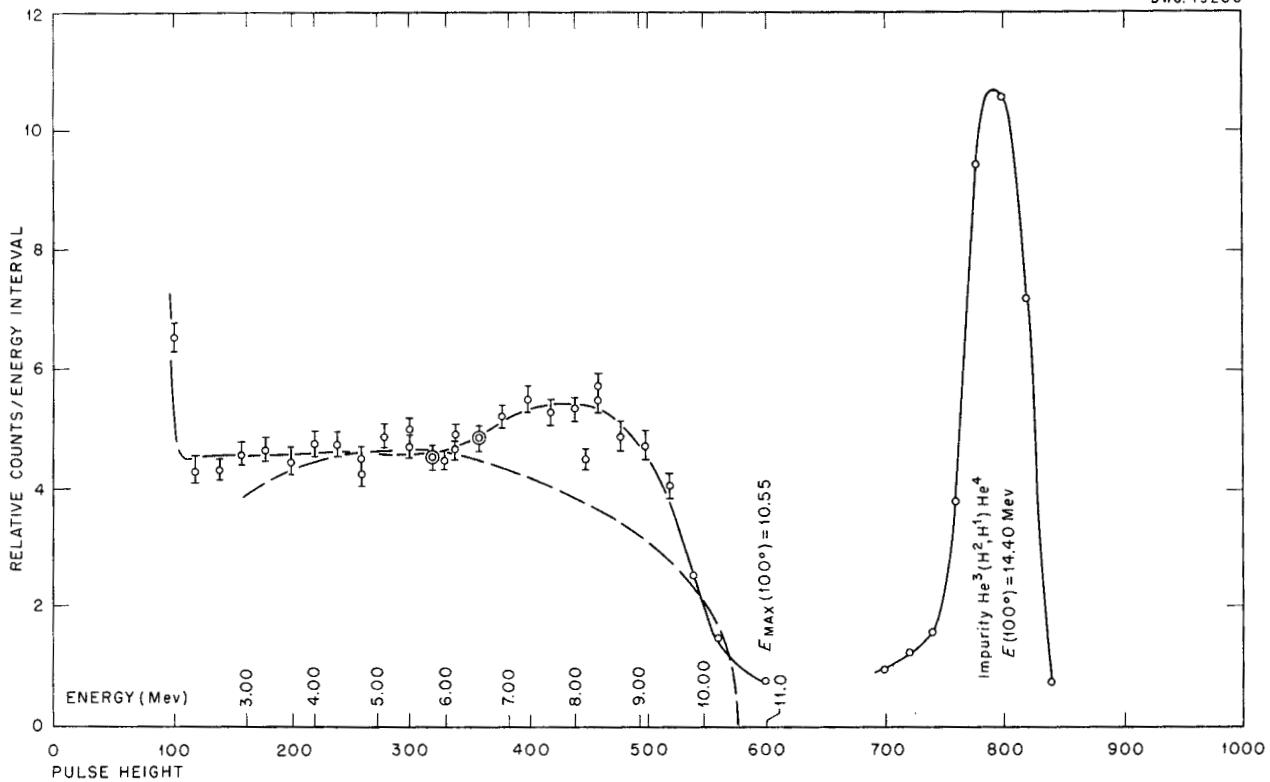


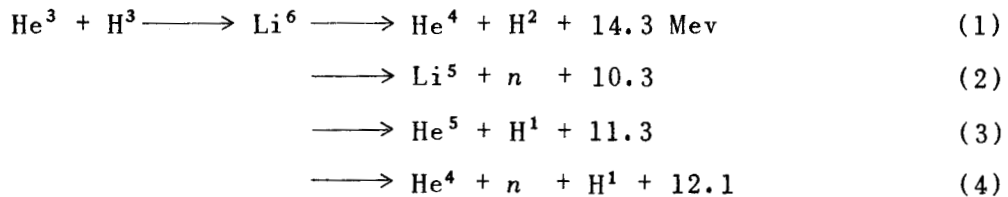
Fig. 1.2. Energy Spectrum of Protons in the Reactions $\text{He}^3 \left[\begin{matrix} \text{He}^3, & \text{Li}^5 \\ & \text{He}^4, \text{H}^1 \end{matrix} \right] \text{H}^1$.

competing three-body breakup. On the basis of a simple statistical proton energy distribution for the three-body breakup, an energy range of 1.8 to 2.2 Mev results for the position of the level in Li^5 relative to an alpha particle and a free proton.

ENERGY SPECTRUM OF PARTICLES FROM H^3
BOMBARDED BY He^3

C. D. Moak W. M. Good

The following modes of decay are expected to follow the capture of He^3 by H^3 :



Almqvist *et al.*⁽²⁾ have identified reactions 1, 3, and 4. Reaction 3 affords an opportunity to look for the levels in He^5 ; consequently this reaction was re-examined by using the target arrangement shown in Fig. 1.3. The target consisted of approximately 100 μg of zirconium tritide. With a 3- μa He^{3+} beam and a bombarding energy of 360 keV, the counting rates were sufficiently large to permit 3% counting statistics. The beam was monitored by counting all pulses greater in height than the pulses from the alpha recoils in reaction 1.

Figure 1.4 shows the energy spectrum of particles obtained by using the geometry of Fig. 1.3. There is little evidence of structure that can be interpreted to confirm levels in He^5 in the proton energy range of 2.5 to 7.5 MeV. However, the deuteron peak definitely shows more width than was

expected. To investigate the deuteron peak further a target arrangement similar to Fig. 1.3 was used, and provision was made for inserting absorbers in front of the detecting crystal. Since deuterons lose energy approximately twice as fast as protons of the same energy, the insertion of absorbers should partially resolve the deuterons and protons that coincide in energy. Figure 1.5 shows the effect of absorbers on the high-energy end of the spectrum. It will be seen that there is a well-defined group of protons corresponding to reaction 3.

GAMMA RAYS FROM PROTON BOMBARDMENT OF LIGHT ELEMENTS

C. W. Snyder G. P. Robinson

The circuitry for corona control of the energy of the 2-MeV Van de Graaff accelerator and a nuclear fluxmeter for measuring the field of the analyzing magnet has been installed, and it is now possible to produce proton beams of accurately known energy homogeneous to a few kilovolts. Thus the 5.2-keV wide gamma-ray resonance in fluorine at 873.5 keV was found on one occasion to have an observed width of 7.3 keV, which indicated a resolution of about 5 keV (0.6%) for the accelerator.

Gamma rays resulting from proton bombardment of C^{13} , N^{15} , and Li^6 were investigated by using a NaI crystal scintillation spectrometer. No gamma ray of the energy to be expected from proton capture was observed with Li^6 up to 1.8 MeV, but the Li^7 gammas made it impossible to determine the upper limit of the cross section. Much purer Li^6 (less than 1% Li^7) would be desirable for this experiment.

A previously unreported resonance for the reaction $\text{N}^{15}(p, \alpha, \gamma)\text{C}^{12}$ was found at a bombarding energy of 1646 ± 10 keV with a width of approximately 75 keV. The C^{12} nucleus is

(2) E. Almqvist, K. W. Allen, J. T. Dewan, and T. P. Pepper, " $\text{He}_4 + \text{T}$ Reactions," *Bull. Am. Phys. Soc.* 26, No. 3, 11 (1951).

UNCLASSIFIED
DWG. 15201

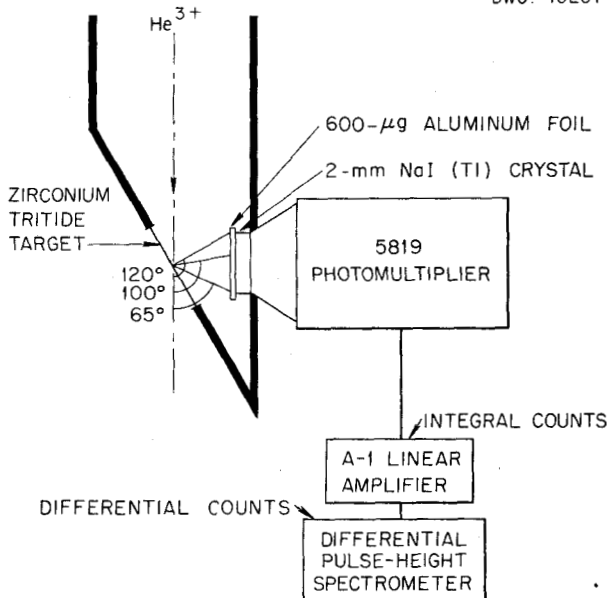


Fig. 1.3. Apparatus for Bombardment of H^3 by He^3 .

PHYSICS DIVISION QUARTERLY PROGRESS REPORT

UNCLASSIFIED
DWG. 15202

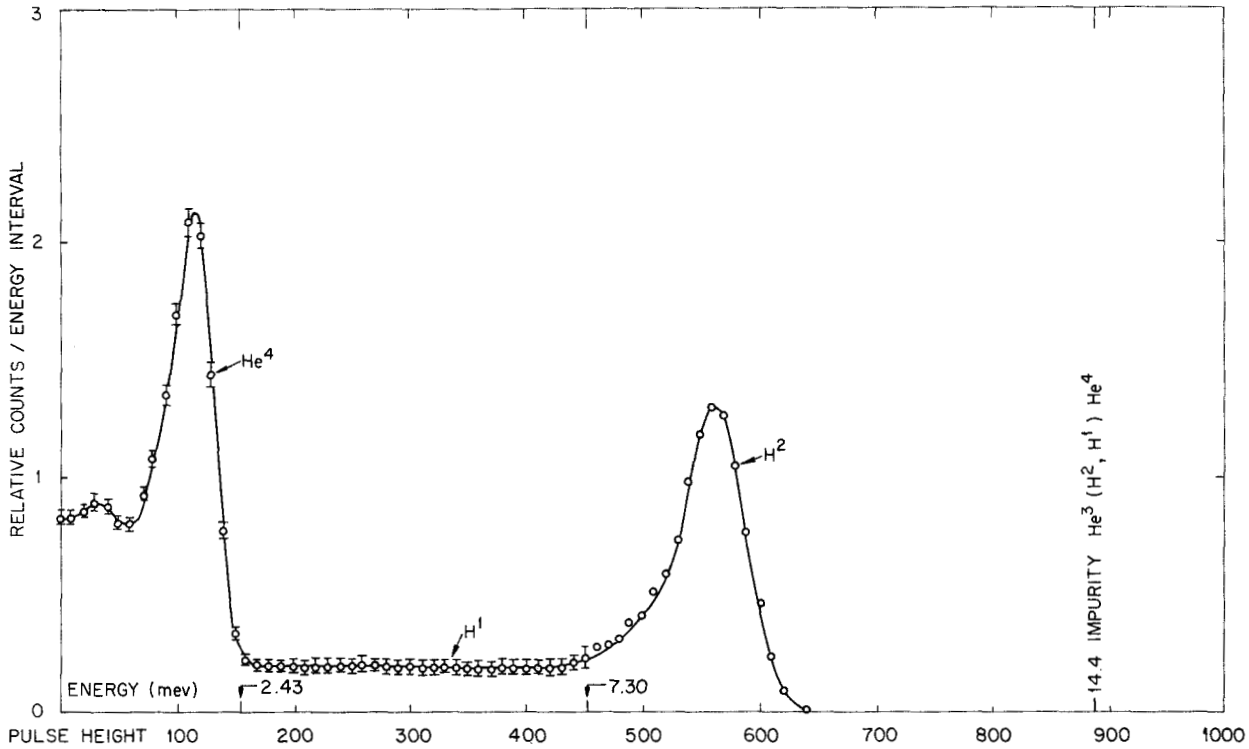


Fig. 1.4. Energy Spectrum of Particles Accompanying Breakup of Li^6 Formed by He^3 Capture on H^3 .

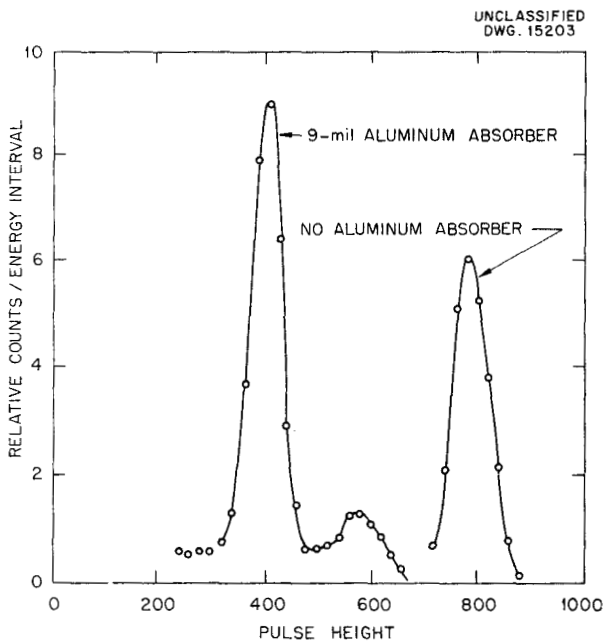


Fig. 1.5. Energy Spectrum of Particles from $\text{He}^3 + \text{H}^3$ Reaction With and Without Aluminum Absorber.

left in the 4.47-Mev excited state, as is the case with the lower energy resonances. The resonance previously reported⁽³⁾ at 1.21-Mev proton energy has been observed at 1215 ± 3 kev. Some indications of resonances in $\text{N}^{15}(p, \gamma)\text{O}^{16}$ were found above 1.0 Mev, and this search is being continued.

The pulse-height spectrum of the gamma rays from the 1.76-Mev resonance in $\text{C}^{13}(p, \gamma)\text{N}^{14}$ was studied. In addition to the 9.175-Mev gamma ray to the ground state,⁽⁴⁾ gamma rays of energies 6.44, 2.73, 6.93, and 2.25 Mev were found. Apparently there are other gamma rays, so this investigation will be continued.

(3) A. W. Schardt, W. A. Fowler, and C. C. Lauritsen, "Transmutation of N^{15} by Protons," *Phys. Rev.* **80**, 136 (1950).

(4) H. H. Woodbury, R. B. Day, and A. V. Tellestrup, "Measurement of Gamma-Rays in the Reaction $\text{C}^{13}(p, \gamma)\text{N}^{14}$," *Phys. Rev.* **85**, 760 (1952).

INELASTIC SCATTERING

H. B. Willard J. K. Bair
J. D. Kington

Measurements of the type previously reported for iron⁽⁵⁾ have been continued for boron, fluorine, aluminum, and magnesium. Similar discontinuities occur in the gamma-ray response curves as a function of neutron energy, but it is not yet certain whether it is proper to associate these breaks with energy levels excited in the bombarded nucleus by inelastic neutron scattering.

THE $H^3(p, \gamma)He^4$ REACTION

J. K. Bair H. B. Willard
J. D. Kington

Preliminary measurements of the yield of 20-Mev gamma rays from the proton bombardment of tritium have been made by using a NaI (Tl) scintillation counter biased above 10 Mev. The yield from 1 to 5 Mev exhibits a general rise with no evidence for the maximum at 3 Mev observed in the $H^3(p, n)He^3$ reaction.

THE $C^{13}(p, n)N^{13}$ REACTION

J. K. Bair H. B. Willard
J. D. Kington

The yield of the $C^{13}(p, n)N^{13}$ reaction in the forward direction has been measured from threshold (3.236 Mev)⁽⁶⁾ to 5 Mev. Neutrons were detected with a long counter placed at zero degrees with respect to the proton beam and at a distance of 60 cm from the target. The target consisted of a thin layer (approximately 4 kev at threshold) of carbon on platinum.

⁽⁵⁾ J. K. Bair, H. B. Willard, C. H. Johnson, and J. D. Kington, "Inelastic Scattering of Neutrons by Elemental Iron," *Physics Division Quarterly Progress Report for Period Ending December 20, 1951*, ORNL-1278, p. 4.

⁽⁶⁾ H. T. Richards and R. V. Smith, "P-N Thresholds for Calibration Points on the Nuclear High Voltage Scale," *Phys. Rev.* **77**, 752 (1950).

Targets were prepared by H. E. Banta by cracking methyl iodide vapor (enriched to 61% C^{13} and obtained from Eastman Kodak Co.). Proton energy calibration was accurate to 0.2% relative to the $Li^7(p, n)Be^7$ threshold at 1.882 Mev, whereas the resolution used was somewhat better than 0.2%.

Figure 1.6 shows the unnormalized results of several runs. Maximums in the yield were found at 3.78, 4.01, 4.19, 4.53, and 4.78 Mev, which correspond to N^{14} excitation energies of 11.05, 11.26, 11.43, 11.75, and 11.98 Mev. The level at 3.78 Mev has been previously observed.⁽⁷⁾

THE $B^{11}(p, n)C^{11}$ ANGULAR DISTRIBUTION

H. B. Willard J. K. Bair
J. D. Kington

The angular distribution of neutrons from the reaction $B^{11}(p, n)C^{11}$ has been studied from threshold (3.015 Mev)⁽⁶⁾ to 5 Mev. A thin (50 kev at 3 Mev) target of natural boron was bombarded with the analyzed beam of protons from the 5.5-Mev Van de Graaff, and the neutrons were detected with a long counter located at a distance of 1 meter. Absolute cross sections were obtained by calibration of this counter with a standard polonium-beryllium source. Since the flatness of response of the long counter has not been determined, this method is believed accurate to only $\pm 10\%$.

Figure 1.7 shows the yield of neutrons emitted in the forward direction (laboratory system). Definite resonances are observed at 3.14, 3.55, and 4.65 Mev with level widths of 80, 400, and 200 kev, respectively. A flat region between 4.0 and 4.4 Mev is resolved into two levels when observed

⁽⁷⁾ R. E. Adamson, Jr., W. W. Buechner, W. M. Preston, C. Goodman, and D. M. Van Patter, "The Neutron Yield from the $C^{13}(p, n)N^{13}$ Reaction," *Phys. Rev.* **80**, 985 (1950).

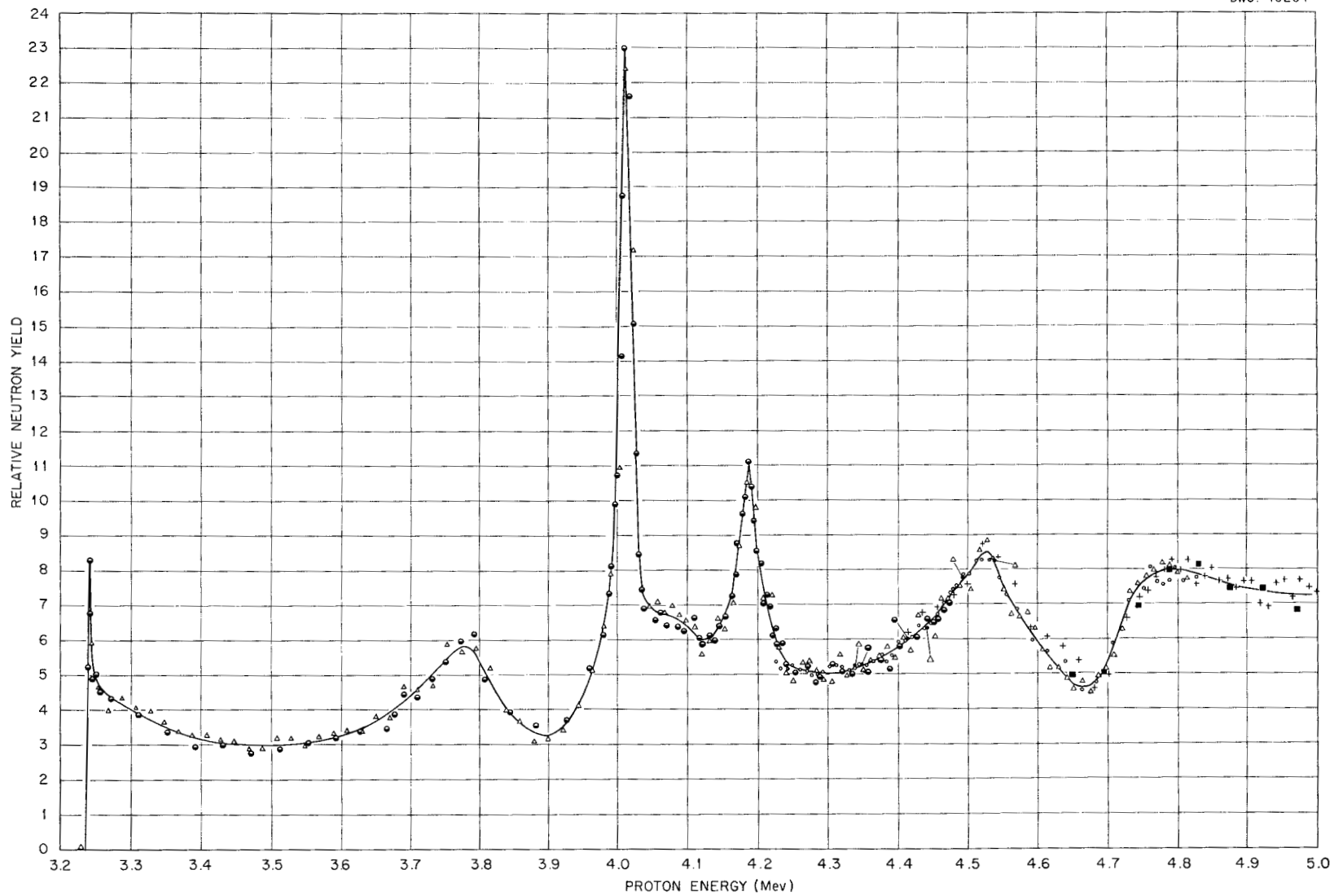


Fig. 1.6. Yield of the $C^{13}(p,n)N^{13}$ Reaction in the Forward Direction.

UNCLASSIFIED
DWG. 15235

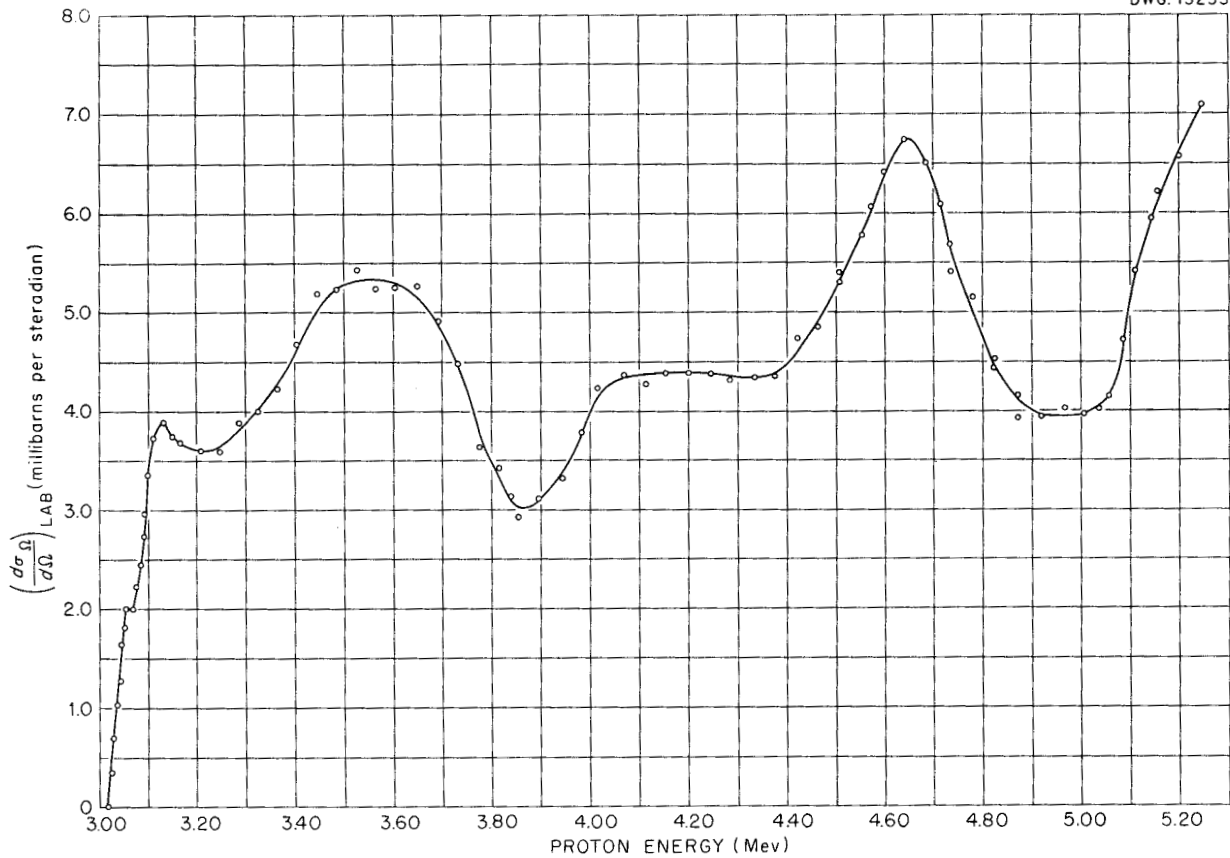


Fig. 1.7. Yield of the $B^{11}(p,n)C^{11}$ Reaction at $\theta_{lab} = 0^\circ$.

at angles greater than zero degrees. Measurements were also taken at laboratory angles of 7.5, 15.0, 22.5, 30, 60, 90, and 120 degrees.

(p,n) THRESHOLDS IN NEON

J. D. Kington H. B. Willard
C. H. Johnson

The (p,n) thresholds in two isotopes of neon have been determined by bombarding a gas target of spectroscopically pure gas with protons and detecting the neutrons with a Bonner-type counter. The $Ne^{21}(p,n)Na^{21}$ reaction has a threshold of 3.944 Mev, which places the Q value at -3.765 Mev.

By using this value and the (n-p)⁽⁸⁾ mass difference, $Na^{21}-Ne^{21}$ is calculated to be 0.00320 amu (atomic mass unit), and therefore the mass of Na^{21} is 21.00360 amu.⁽⁹⁾

The $Ne^{22}(p,n)Na^{22}$ reaction has a threshold of 4.091 Mev, which gives a Q value of -3.913 Mev. Accordingly, the $Na^{22}-Ne^{22}$ mass difference was found to be 0.00336 amu. The mass of Na^{22} is 22.00169 amu.

⁽⁸⁾C. W. Li, W. Whaling, W. A. Fowler, and C. C. Lauritsen, "Masses of Light Nuclei from Nuclear Disintegration Energies," *Phys. Rev.* **83**, 512 (1951).

⁽⁹⁾H. Ewald, "Die Massen der Substandards H^1 , D^2 , C^{12} und anderer leichter Atome," *Z. Naturforsch.* **6a**, 293 (1951).

PHYSICS DIVISION QUARTERLY PROGRESS REPORT

Proton energies were measured relative to the $F^{19}(p,n)Ne^{19}$ threshold at 4.253 Mev⁽¹⁰⁾ and are believed to be accurate to ± 0.010 Mev.

The thick target neutron yield from gold was also studied and was found to

be less than any other material tested to date (tantalum, tungsten, lead, and platinum).

⁽¹⁰⁾H. B. Willard, J. K. Bair, J. D. Kington, T. M. Hahn, C. W. Snyder, and F. P. Green, "The Yield of Gamma-Rays and Neutrons from the Proton Bombardment of Fluorine," *Phys. Rev.* **85**, 849 (1952).

2. RADIOACTIVITY AND NUCLEAR ISOMERISM

ANGULAR CORRELATION OF GAMMA RAYS

E. D. Klema G. B. Arfken
F. K. McGowan

The work on the angular correlation of the gamma rays emitted by Pd^{106} has been completed and is to appear in the May 1 issue of *The Physical Review*.

The correlations of the gamma rays from Ba^{134} have been investigated under several experimental conditions, but the results cannot yet be properly interpreted because the decay scheme is now in doubt. The decay scheme shown in NBS-499⁽¹⁾ and that proposed by Schmidt and Keister⁽²⁾ are inconsistent with the results obtained in the present experiments. Coincidences between the 0.794-Mev gamma rays and radiation of energy greater than 0.794 Mev have been observed that are not predicted by the decay scheme given in NBS-499. Coincidences between the 1.35-Mev gamma rays and the 0.561- or 0.601-Mev gamma rays have also been observed, but they should not exist according to the decay scheme of Schmidt and Keister.

The angular correlation of the gamma rays emitted in the decay of excited states in Cd^{114} is presently

being investigated. The correlation has been measured with one analyzer set on the photopeak of the 0.715-Mev gamma ray and the other detector set on the photopeak of the 0.548-Mev gamma ray and with both detectors set to include both photopeaks. It has been shown that the observed correlation is not affected by the positrons emitted in the decay of In^{114} in the first experiment described previously and that the results obtained in the second arrangement show this effect. The intensity of the 1.27-Mev crossover gamma ray has been measured and was found to be approximately 6%.

The apparatus has been checked by measuring the ratio of coincidence counting rates at 180 and 90 deg with two experimental arrangements that use the gamma rays of Co^{60} . In one experiment each detector was set to count all pulses above the lower edge of the photopeak of the 1.17-Mev gamma ray; in the other experiment each detector was set to count pulses corresponding to energies greater than 0.7 Mev. The same ratios were obtained in the two experiments.

GAMMA-GAMMA ANGULAR CORRELATIONS IN Ta^{181}

F. K. McGowan

The directional angular correlation of several gamma-ray cascades in Ta^{181} that follow the beta decay of Hf^{181} has been measured with a coincidence

⁽¹⁾National Bureau of Standards Nuclear Data, NBS-499 (Sept. 1, 1950).

⁽²⁾F. H. Schmidt and G. L. Keister, "The Beta-Spectrum of 2.3-Year Cs^{134} ," *Bull. Am. Phys. Soc.* **27**, No. 1, 57 (1952).

scintillation spectrometer employing NaI detectors. The correlation of the 132-keV gamma ray with the 480-keV gamma ray is anisotropic. For sources of normal HfO₂ the measured anisotropy

$$\epsilon = \frac{W(\pi) - W\left(\frac{\pi}{2}\right)}{W\left(\frac{\pi}{2}\right)} = -0.15 .$$

Since the intermediate state is metastable with $T_{1/2} = 10^{-8}$ sec, the true anisotropy is at least this large. The initial state of the 132-keV transition is the well-known 22- μ sec isomeric state, and the measured *K*-shell internal conversion coefficient indicates that the transition is an *E2*. The 480-keV transition is probably *E2*, based on lifetime considerations, although the transition is considerably slower than that expected from the one-particle model. The observed anisotropy fails to fit any one of the following 24 sequences:

$j, j \pm 1, j \pm 2 \xrightarrow{E2} j = 7/2, 7/2 \pm 1, 7/2 \pm 2 \xrightarrow{E2} 7/2$. Also, the following mixed multipoles for the sequences $1/2(E2)5/2(E2,M1)7/2$ and $1/2(E2,M1)3/2(E2)7/2$ with the *M1* intensity small compared to *E2* fail to explain the experimental observation.

The combined correlations of the 132-keV gamma ray with the 344-keV gamma ray and the 344-keV gamma ray with the 135-keV gamma ray are anisotropic with $\epsilon = 0.08$. The one-three gamma-gamma angular correlation of the 132-keV gamma ray with the 135-keV gamma ray is also slightly anisotropic with $\epsilon = -0.04$. Since the level 480 keV above the ground state is metastable, and Hf¹⁷⁵ (70-day) is present in sources of normal hafnium, the interpretation of the latter correlations is being withheld until the experiments are repeated with the separated isotopes.

K-SHELL INTERNAL CONVERSION COEFFICIENT MEASUREMENTS

F. K. McGowan

K-shell internal conversion coefficients have been measured for gamma-ray transitions in La¹³⁹ and Te¹²³. The intensity ratio of the *K* x ray to the gamma ray is obtained from a spectral measurement of the gamma radiation with a NaI scintillation spectrometer. The experimental and theoretical internal conversion coefficients are tabulated in Table 2.1.

For the 165-keV transition in La¹³⁹ it is impossible to distinguish between *E2* and *M1* radiation from a

TABLE 2.1

Experimental and Theoretical Internal Conversion Coefficients

NUCLEUS	<i>E_γ</i> (keV)	<i>T</i> _{1/2} (sec)	<i>K/L</i>	α_{exp}^K	THEORETICAL	
					α_2^K	β_1^K
La ¹³⁹	165	$< 4 \times 10^{-8}$	6 ⁽³⁾	0.28 ± 0.03	0.254	0.253
Te ^{123*}	159	$< 10^{-9}$	8.6 ⁽⁴⁾	0.19 ± 0.02	0.260	0.175

(3) L. R. Shepherd and J. M. Hill, "Decay of Barium-139," *Nature* **162**, 566 (1948).

(4) R. D. Hill, "The Absence of Cross-Over Transitions in Tellurium Isomers," *Phys. Rev.* **81**, 470 (1951).

PHYSICS DIVISION QUARTERLY PROGRESS REPORT

measurement of the K -shell conversion coefficient. However, the K/L ratio lends support to the assignment of $M1$ or $(M1 + E2)$ for the transition. These data fit very well with the prediction of the spin-orbit coupled shell model. The suggested level assignment is $d_{5/2} \longrightarrow g_{7/2}$.

The 159-keV transition of Te^{123} is preceded by the well-known $M4$ transition of 88 keV. To obtain the spectrum of the gamma radiation associated with the 159-keV transition it is necessary to measure the spectrum in coincidence with only the L and M conversion electrons from the $M4$ transition. The data indicate that the transition is predominantly $M1$ in agreement with the shell model prediction, which is $d_{3/2} \longrightarrow s_{1/2}$. The data do not

exclude an admixture of $E2$. A sensitive test for this would be a measurement of the directional angular correlation of the gamma-gamma cascade. For instance, an intensity ratio of $E2$ to $M1$ of 1% changes the anisotropy $[-0.21$ for the sequence $11/2(M4)3/2(M1)1/2]$ by $\pm 30\%$ depending on the sign of the amplitude ratio of the multipoles present in the mixture. Since the $M4$ transition is almost totally converted, the only angular correlation measurement possible is the e^- -gamma, for which the predicted anisotropy⁽⁵⁾ is a few per cent larger than the gamma-gamma anisotropy. An attempt is being made to measure the e^- -gamma anisotropy.

⁽⁵⁾ M. E. Rose, L. C. Biedenharn, and G. B. Arfken, "Internal Conversion Angular Correlations," *Phys. Rev.* **85**, 5 (1952).

3. NEUTRON DIFFRACTION

NEUTRON DIFFRACTION STUDIES ON SUPERCONDUCTING ELEMENTS

C. G. Shull T. E. Stephenson
M. K. Wilkinson S. Bernstein
L. D. Roberts

Previous work on the determination of the magnetic structure existing in various transition elements including molybdenum, vanadium, niobium, and chromium had involved their examination at temperatures as low as that of liquid hydrogen (20°K). Since some of these elements become superconducting at temperatures in the vicinity of liquid helium, it was decided to examine several of them while they were in the superconducting state. It was thought that the electronic ordering that presumably accompanies the formation of the superconducting state might show itself in the neutron diffraction pattern either in the form of extra coherent features or possibly as an altered diffuse scattering. A

second point of interest lay in the determination of the lattice characteristic temperature above and below the superconducting transition to see if the large changes in specific heat variation are to be accounted for by lattice vibration effects.

The samples were in the form of filings or loosely packed powder sealed with a helium atmosphere in an aluminum-walled capsule. The top part of the sample tube was in direct thermal contact with the coolant reservoir (liquid helium or hydrogen), and to ensure that the sample was in a superconducting state, a small coil was mounted around the bottom end of the sample tube. A pronounced change in mutual inductance between this coil and a primary coil mounted outside the cryostat occurred when the sample was cooled through its superconducting transition because of the magnetic field ejection by a superconductor.

Neutron diffraction patterns were taken at temperatures of 4.1 and 20.4°K for three materials, vanadium, lead, and niobium, whose superconducting transition temperatures are 4.7, 7.2, and 8.7°K, respectively. In no case was there observed (1) any extra coherent scattering features either at new reflection positions or superimposed on the normal nuclear scattering pattern, or (2) any measurable change in the diffuse scattering. Vanadium samples are particularly useful in the search for effects of type (1) since there are no interfering nuclear reflections, whereas lead and niobium are more significantly used in a search for diffuse scattering effects. Thus no electronic scattering effects have been observed either of a coherent or an incoherent nature.

In addition to the observations on possible electronic scattering by the superconducting lattice, the normal nuclear reflections have been studied to see if there existed any abnormal change in intensity in going through the superconducting transition. All of the observed reflections for lead and niobium appeared to have a normal temperature dependence as described quantitatively by the Debye-Waller theory with little or no change in lattice characteristic temperature. Specific heat observations in niobium show drastically different temperature behavior above and below the superconducting transition at 8.7°K, and these are usually described in terms of different characteristic temperatures, θ_n and θ_s , for the normal and superconducting lattices. For niobium, θ_n and θ_s are respectively⁽¹⁾ 254 and 161°K. Such a change in lattice characteristic temperature should have been observable in the nuclear reflections of niobium; for instance,

the (310) intensity should have changed by -3.4% in cooling from 20.4 to 4.1°K, whereas two different determinations gave -0.5 and +0.7%. With no change in characteristic temperature in passing through the superconducting temperature, the expected change is +0.3%. Thus the neutron scattering data suggest that there is no pronounced change in the atomic lattice vibrations above and below the superconducting transition.

NEUTRON DIFFRACTION STUDIES OF SOME RARE EARTHS

W. C. Koehler E. O. Wollan

A report was given in the last quarterly⁽²⁾ on measurements of the coherent and total neutron cross sections of lanthanum, cerium, praseodymium, and neodymium and of some of the separated isotopes of cerium and neodymium. In addition it was found possible from the neutron measurements to determine unambiguously the structure of the sesquioxides of the type La_2O_3 .

The cross-section studies have now been extended to include a separated isotope of samarium (Sm^{152}), and a sample of Sm^{154} is now being investigated. The very large capture cross section of normal samarium (associated with Sm^{149}) makes it impossible to investigate by the neutron diffraction technique. Even with the sample enriched in Sm^{152} the absorption cross section amounted to about 900 barns per Sm_2O_3 molecule, about half of which is due to Sm^{152} and the remainder is due to Sm^{149} .

In spite of the large capture and the complicated unit cell associated

(1) A. Brown, M. W. Zemansky, and H. A. Boorse, "Low Temperature Heat Capacity of Niobium," *Bull. Am. Phys. Soc.* **27**, No. 1, 52 (1952).

(2) W. C. Koehler and E. O. Wollan, "Neutron Scattering Studies of the Light Rare Earths," *Physics Division Quarterly Progress Report for Period Ending December 20, 1951*, ORNL-1278, p. 12.

PHYSICS DIVISION QUARTERLY PROGRESS REPORT

with the Sm_2O_3 structure, it was possible to obtain a value for the Sm^{152} nuclear scattering amplitude. This isotope has a negative scattering phase, the value of the coherent amplitude is $f_{coh} = -0.45 \pm 0.05 \times 10^{-12}$, and the corresponding cross section σ_{coh} is approximately 2.5 barns.

The neutron scattering studies of the rare-earth oxides were initiated primarily for the purpose of obtaining information about their magnetic scattering properties. The effective magnetic moment of the trivalent rare-earth ions as determined from susceptibility measurements is comparable and in the heavy group even larger than the moments encountered in the iron group. An appreciable amount of paramagnetic scattering might be expected from these rare-earth ions.

Measurements have now been made of the coherent and diffuse scattering by the oxides of neodymium and praseodymium for scattering angles as small as 3 deg at room temperature and also at liquid nitrogen and liquid hydrogen temperatures. No angularly dependent paramagnetic or other magnetic scattering effects have been observed within the accuracy of the measurements, although the sensitivity of the measurements would be sufficient to detect a small fraction of the scattering that would be present if the magnetic moment values obtained from susceptibility measurements contributed directly to the scattering.

It is planned in the near future to obtain information about the heavy group by studying a sample of erbium, which has been loaned by G. E. Boyd of the ORNL Chemistry Division. The theoretical significance of these results can be more profitably considered when more complete data are available.

MAGNETIC STRUCTURE OF Mn_2Sb

N. S. Gingrich C. G. Shull

The neutron diffraction pattern of a powdered sample of Mn_2Sb is being studied to make a direct determination of the arrangement and disposition of the magnetic manganese ions in this crystal. The structure of the crystal as determined earlier by x rays gives not only the type of crystal but also the locations of the manganese and antimony atoms in the unit cell. Nevertheless, the neutron diffraction pattern of this material shows marked differences in the intensities of many reflections as compared with those obtained with x rays. It is believed that these differences may be inherent in the methods of obtaining the diffraction patterns: with x rays there is no scattering as a result of the magnetic moments of any of the ions in the crystal, whereas with neutrons the magnetic scattering may be very important. From an analysis of the neutron scattering it is to be expected that direct information can be obtained regarding the magnetic structure of the crystal and the orientation of the elementary magnetons.

The neutron diffraction pattern of powdered Mn_2Sb obtained at room temperature has been plotted, corrected for (1) scattering by the empty cell, (2) absorption in the sample, and (3) second-order contamination in the radiation, and placed on an absolute basis by means of a calibration run with nickel. Values of the integrated reflections for nine peaks in the experimental curve have been determined. From known values for the nuclear cross sections of manganese and antimony, numerical values of the intensities caused by nuclear scattering have been calculated for 34 reflections from the Mn_2Sb lattice.

By using the model for the location and orientation of the magnetic moments of the manganese ions as proposed by Guillaud from macroscopic magnetic measurements, intensities have been calculated for the magnetic scattering for the same 34 reflections. Intensities caused by magnetic scattering have been calculated for three other models of magnetic structure for several of the important reflections, and comparisons with experimentally determined values favor Guillaud's model. Refinements in the calculation of intensities are now being made to include the effect on these intensities of the lattice vibrations, and preparations are under way to obtain patterns for different conditions of temperature and for the magnetic field.

TOTAL NEUTRON CROSS SECTIONS AT INDIUM RESONANCE ENERGY (1.44 ev)

L. A. Rayburn E. O. Wollan

Total free-scattering cross sections can be obtained from transmission measurements at indium resonance energy (1.44 ev) for those cases for which capture is negligible or for which capture is small and quite accurately known from pile oscillator measurements. In a previous quarterly report⁽³⁾ some measurements were recorded, and they are extended here in Table 3.1.

⁽³⁾L. A. Rayburn and E. O. Wollan, "Total Neutron Cross Sections at Indium Resonance Energy (1.44 ev)," *Physics Division Quarterly Progress Report for Period Ending September 20, 1951*, ORNL-1164, p. 34.

TABLE 3.1

Cross Sections at 1.44 ev

SAMPLE	σ_{total} (barns)	σ_c (0.025 ev) (Pile oscillator measurements by H. Pomerance)	σ_c (1.44 ev) (barns)	σ_s (barns)
H ₂ O	46.1 ± 0.3			
D ₂ O	10.6 ± 0.1			
Carbon (diamond dust)	4.7 ± 0.1			4.7 ± 0.1
Aluminum	1.45 ± 0.01	0.22 ± 0.01	0.03	1.42 ± 0.01
Vanadium	5.4 ± 0.1	4.7 ± 0.2	0.62	4.8 ± 0.2
Fe ⁵⁶	12.6 ± 0.2	2.55 ± 0.13	0.34	12.3 ± 0.2
Ni ⁵⁸	24.2 ± 0.2	4.23 ± 0.2	0.55	23.6 ± 0.2
Magnesium	3.35 ± 0.05	0.06 ± 0.01	0.01	3.34 ± 0.05
Lead	11.30 ± 0.05	0.19 ± 0.01	0.03	11.27 ± 0.05

PHYSICS DIVISION QUARTERLY PROGRESS REPORT

4. LOW-TEMPERATURE PHYSICS

SPECIFIC HEAT OF NEODYMIUM ETHYL SULFATE FROM 1 TO 2°K

L. D. Roberts C. C. Sartain

The theory and preliminary results of the measurement of the specific heat of $\text{Nd}(\text{C}_2\text{H}_5\text{SO}_4)_3 \cdot 9\text{H}_2\text{O}$ in the temperature region from 1 to 2°K were presented in a previous quarterly report.⁽¹⁾ Since that time the apparatus has been improved by the installation of an oil-cooled solenoid capable of giving larger magnetic fields,⁽²⁾ H (approximately 1000 gauss), and results of much greater precision have been obtained.

Materials Used. Three neodymium ethyl sulfate samples having different isotopic compositions of neodymium (Table 4.1) were measured. The samples were spherical in shape, weighed about

1 g each, and were prepared by compressing powdered crystals (approximately 1 mm³) of the salt into a spherical 1.2-cm-ID lucite container. The compression was to about 80% of the crystal density. Each sample was recrystallized twice, and the last recrystallization was performed immediately before the low-temperature measurements were made.

Results. Measurements of the parameter b/C , the ratio of the specific heat constant, b , to the curie constant, C ($b = C_I/T^2$, where C_I is the specific heat at constant magnetization and T is the absolute temperature), were made as described previously.⁽¹⁾ Measurements on the three samples were carried out at 180, 300, 600, 900, and 1200 cycles/sec at a number of temperatures (Table 4.2), and the value listed for a given temperature is the average result for these five frequencies.

The values for the specific heat constant, b , were obtained by multiplying the average value of b/C for

(1) L. D. Roberts, C. C. Sartain, and J. W. T. Dabbs, Jr., "Specific Heat of Neodymium Ethyl Sulfate and of Neodymium Sulfate from 1 to 2°K," *Physics Division Quarterly Progress Report for Period Ending September 20, 1951*, ORNL-1164, p. 44.

(2) Equation 1, *op. cit.*, ORNL-1164, p. 44.

TABLE 4.1

Isotopic Composition of the Neodymium Used To Prepare the Samples

ISOTOPE	ABUNDANCE (%)		
	Sample I (normal)	Sample II	Sample III
142	27.13	4.04	93.00
143	12.20	83.93	3.18
144	23.87	8.83	2.89
145	8.30	1.78	0.368
146	17.18	1.16	0.414
148	5.72	0.149	0.084
150	5.60	0.108	0.066

TABLE 4.2

Measurements of b/C on Three Neodymium Samples

T ($^{\circ}\text{K}$)	$b/C \times 10^{-5}$ ^(a)		
	SAMPLE I	SAMPLE II	SAMPLE III
2.155		6.81	
2.15			0.4807
2.145	1.363		
1.64			0.4761
1.630		6.62	
1.450		6.64	
1.39			0.4662
1.122	1.361		
1.121		6.70	
1.10			0.4767
1.000	1.377		
0.97			0.4724
0.95		6.72	
Average	1.367	6.70	0.4744
Weiss $\theta = 0.013 \pm 0.005^{\circ}\text{K}$			

^(a)Average value for five frequencies.

each of the three salts by the Curie constant per mole ($C = 0.663$) for the powder as calculated from the microwave measurements by Scovil⁽³⁾ and the measurements by Van den Handel and Hupse.⁽⁴⁾ For sample I, the normal neodymium sample, $b = 0.906 \times 10^5$ erg·deg; for sample II, Nd^{143} , $b = 4.44 \times 10^5$ erg·deg; and for sample III, Nd^{142} , $b = 0.3145 \times 10^5$ erg·deg. If these values of b are collected in

the corresponding simultaneous equations, it is then possible to solve for the three contributions to the specific heat: (1) b_e , the specific heat constant owing to electron-electron interaction; (2) b_3 , the specific heat constant corresponding to the Nd^{143} hyperfine splitting; and (3) b_5 , the specific heat constant corresponding to the Nd^{145} hyperfine splitting. These equations and the values of b_e , b_3 , and b_5 are summarized in Table 4.3.

⁽³⁾Proceedings of the International Conference on Low Temperature Physics, R. Bowers, ed., Clarendon Laboratory, Oxford, 1951.

⁽⁴⁾J. v. d. Handel and J. C. Hupse, "The Magnetic Susceptibilities of a Single Crystal of Neodymium-ethylsulfate," *Physica* 9, 225 (1942).

These values of b agree within experimental error with the values $b_3 = 5.17 \times 10^5$ erg·deg and $b_5 = 2.00 \times 10^5$ erg·deg computed from the microwave measurements of Scovil.⁽³⁾ The value

PHYSICS DIVISION QUARTERLY PROGRESS REPORT

TABLE 4.3

Simultaneous Equations for Specific Heats of Neodymium Samples

$4.44 \times 10^5 = b_e + 0.8393b_3 + 0.0178b_5$
$0.906 \times 10^5 = b_e + 0.1220b_3 + 0.0830b_5$
$0.3145 \times 10^5 = b_e + 0.0318b_3 + 0.0037b_5$
$b_3 = 5.08 \pm 0.05 \times 10^5 \text{ erg}\cdot\text{deg}$
$b_5 = 1.7 \pm 0.2 \times 10^5 \text{ erg}\cdot\text{deg}$
$b_e = 0.147 \pm 0.004 \times 10^5 \text{ erg}\cdot\text{deg}$

of $b_e = 0.147 \pm 0.004 \times 10^5$ is one of the smallest electron-electron interactions that has been observed. This results in the unusual circumstance that for $\text{Nd}^{143}(\text{EtSO}_4)_3 \cdot 9\text{H}_2\text{O}$ the hyperfine splitting contribution to the specific heat is some 30 times larger than the electron-electron interaction contribution, which makes this material of considerable interest in the study of nuclear effects below 1°K .

In Table 4.2 a Weiss constant of $0.013 \pm 0.005^\circ\text{K}$ was used in calculating the specific heat. This value is smaller than can be obtained precisely from susceptibility measurements. The value obtained for b_5 without a Weiss constant correction was approximately 4% lower than the corresponding microwave value. Since the precision of the susceptibility and magnetic field measurements was considerably better than 1% it is reasonable to assume that the 4% discrepancy is due to a small Weiss constant and that $\theta = 0.013 \pm 0.005^\circ\text{K}$ is the value necessary to bring the b_5 value into agreement within experimental error with the microwave results. This comparison provides a very sensitive technique for observing a Weiss constant, since the Weiss constant enters into the specific heat measurement at the third power, whereas it only enters

linearly in susceptibility measurements.

Opechowski⁽⁵⁾ has given the relationship

$$\frac{b(\text{exchange})}{R} = \frac{2}{3} \frac{\theta^2}{\nu},$$

where $b(\text{exchange})$ is the specific heat constant caused by the electron exchange interaction, R is the gas constant, and ν is the number of nearest neighbors entering into the exchange process. Taking the values obtained for θ and by assuming a number of nearest neighbors equal to 6, it is then possible to calculate an approximate contribution to b_e caused by exchange. The remainder, $b_e - b(\text{exchange})$, would be due to dipole-dipole interaction. The value, $b(\text{exchange})$ equals approximately $1.6 \times 10^3 \text{ erg}\cdot\text{deg}$, was obtained and is only approximate because of the large uncertainty in the Weiss constant and the uncertainty in the effective number of nearest neighbors in the exchange process.

MEASUREMENT OF THE WEISS CONSTANT IN COPPER POTASSIUM SULFATE

To check the behavior of the apparatus used in the work reported in the previous section, measurements were made of the magnetic susceptibility of copper potassium sulfate at a number of temperatures in the liquid helium region and at a number of frequencies. The results of a measurement at 900 cycles/sec are shown in Fig. 4.1. In the graph, M is the setting of the bridge used in measuring the magnetic susceptibility, T is the absolute temperature, and θ is the Weiss constant. For the correct Weiss constant, the graph should be a straight line. The data are plotted

(5) W. Opechowski, "On the Exchange Interaction in Magnetic Crystals," *Physica* 4, 181 (1937).

for three different values of θ , 0, 0.035, and 0.050°K. It is seen that the best straight line is obtained for $\theta = 0.050^\circ\text{K}$. This salt was previously studied by Benzie and Cooke⁽⁶⁾ who obtained $\theta = 0.035^\circ\text{K}$ and by de Klerk who obtained 0.050°K .⁽⁷⁾ The result reported here is in slightly better agreement with the work of de Klerk than with that of Benzie and Cooke.

(6) R. J. Benzie and A. H. Cooke, "Specific Heats of Some Paramagnetic Salts at Temperatures Near 1°K," *Proc. Phys. Soc. (London)* **A63**, 213 (1950).

(7) D. de Klerk, "The Magnetic and Caloric Behaviour of Copper Potassium Sulfate at Temperatures Below 1°K," *Physica* **12**, 513 (1946).

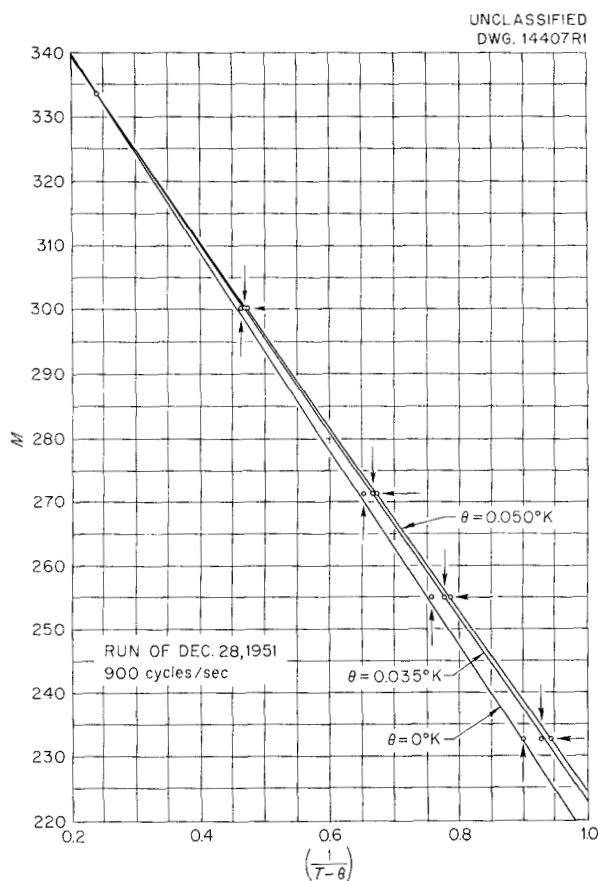


Fig. 4.1. Magnetic Susceptibility of Copper Potassium Sulfate, $\text{CuK}_2(\text{SO}_4)_2 \cdot 6\text{H}_2\text{O}$.

SUPERCONDUCTIVITY OF A HAFNIUM-ZIRCONIUM ALLOY

L. D. Roberts J. W. T. Dabbs

The magnetic susceptibility of a hafnium-zirconium alloy (about 10 at. % zirconium) has been investigated in the liquid helium temperature region and below 1°K by method "a" of Kürti and Simon.⁽⁸⁾ Three metal samples in the form of small chips were studied. Sample I was prepared by the chemical reduction of a mixture of the fluorides with calcium and annealed for 50 hr at 1000°C in a vacuum of about 2×10^{-6} mm. Samples II and III were cut from a "crystal bar" prepared by the hot wire reduction of the iodide. Sample II was not annealed, but sample III was annealed at 785°C for 1½ hr in a vacuum of about 2×10^{-6} mm. About 1 cc of each of these metal samples was pressed with an approximately equal volume of chromium potassium alum, and the magnetic susceptibility of each of the composites was observed by a ballistic method.⁽⁸⁾

Temperatures below 1°K were obtained by adiabatic demagnetization, and the temperatures given in the following text are those of the chromium potassium alum. The thermodynamic temperature was obtained through the use of the $T - T^*$ relationship and from the dependence of the final demagnetization T on the initial H/T as given by de Klerk.⁽⁹⁾ The metal and the salt were undoubtedly in temperature equilibrium at temperatures as low as 0.1°K (Goodman and Mendoza⁽¹⁰⁾) and probably to much lower temperatures. Susceptibility measurements on sample I, in

(8) N. Kürti and F. Simon, "Experiments at Very Low Temperatures Obtained by the Magnetic Method II - New Supraconductors," *Proc. Roy. Soc. (London)* **A151**, 610 (1935).

(9) D. de Klerk, *Onderzoekingen over Adiabatische Demagnetisatie*, Thesis, Leiden, 1948.

(10) B. B. Goodman and E. Mendoza, "The Critical Magnetic Fields of Aluminum, Cadmium, Gallium and Zinc," *Phil. Mag.* **42**, Ser. 7, No. 329, 594 (1951).

PHYSICS DIVISION QUARTERLY PROGRESS REPORT

the temperature region from 0.18 to 4.2°K, and on sample II, in the temperature region from 0.007 to 4.2°K gave no evidence of a superconducting transition. The temperature region below 0.03°K was obtained by using as the coolant salt one part of chromium potassium alum diluted with 13 parts of aluminum potassium alum.⁽⁹⁾ The maximum superconducting volume for samples I and II could not have exceeded 1% and 0.3%, respectively, of the metal volume. Sample III, however, gave a sharp superconducting transition at $0.30 \pm 0.02^\circ\text{K}$ in which effectively the entire volume of the metal became superconducting. This difference of behavior of the three samples probably indicates in the case of hafnium an exceptionally strong dependence of the superconducting transition temperature on annealing and trace impurities (Wexler and Corak⁽¹¹⁾). The value of the superconducting transition temperature of the alloy agrees reasonably with the value, $0.35 \pm 0.05^\circ\text{K}$, previously given for hafnium metal by Kúrti

and Simon.⁽⁸⁾ This problem, which was suggested to us by A. M. Weinberg, was reported at the 1952 New York meeting of the American Physical Society.

Heat Leak Studies Below 1°K. A major problem in the work on adiabatic demagnetization has been the reduction of heat leaks to the cold demagnetized sample or paramagnetic salt. In a previous quarterly report⁽¹²⁾ several sources of heat leak to the sample were discussed, namely, condensation of residual helium gas on the cold (below 1°K) sample and radiation from room temperature through the exchange gas pumping line. It has also been observed that vibration of the cryostat can constitute a large heat leak of the order of hundreds of ergs per minute, which confirms recent work at Oxford. As an outcome of these recent studies, the demagnetization cryostat has been shock-mounted so that the heat leak to the sample is occasionally small - of the order of 10 ergs/min.

⁽¹¹⁾A. Wexler and W. S. Corak, "Superconductivity of Vanadium," *Phys. Rev.* **85**, 85 (1952).

⁽¹²⁾"Heat Leak Studies Below 1°K," *op. cit.*, ORNL-1164, p. 47.

5. HEAVY-ION PHYSICS

SPACE DISTRIBUTION OF IONIZATION IN A GAS

G. E. Evans C. F. Barnett
P. M. Stier V. L. DiRito

The distribution in space of the ionization produced by a collimated beam of heavy ions has been measured for various heavy ions, target gases, and initial energies. The equipment used is shown schematically in Fig. 5.1. The beam of heavy ions enters the large gas chamber via the windowless differential pumping system described in the preceding quarterly report.⁽¹⁾

The pinhole apertures of the differential pumping system also collimate the beam at a diameter of 0.030 inch. The ionization density at any chosen point (R, r) within the gas is measured by using a small ion chamber eccentrically mounted so as to permit lateral and longitudinal motion.

Figures 5.2, 5.3, and 5.4 show the contours of equal ionization density

⁽¹⁾G. E. Evans, C. F. Barnett, P. M. Stier, and V. L. DiRito, "Extrapolated Ionization Ranges of Ions Heavier than Protons," *Physics Division Quarterly Progress Report for Period Ending December 20, 1951*, ORNL-1278, p. 17.

UNCLASSIFIED
DWG. 14740

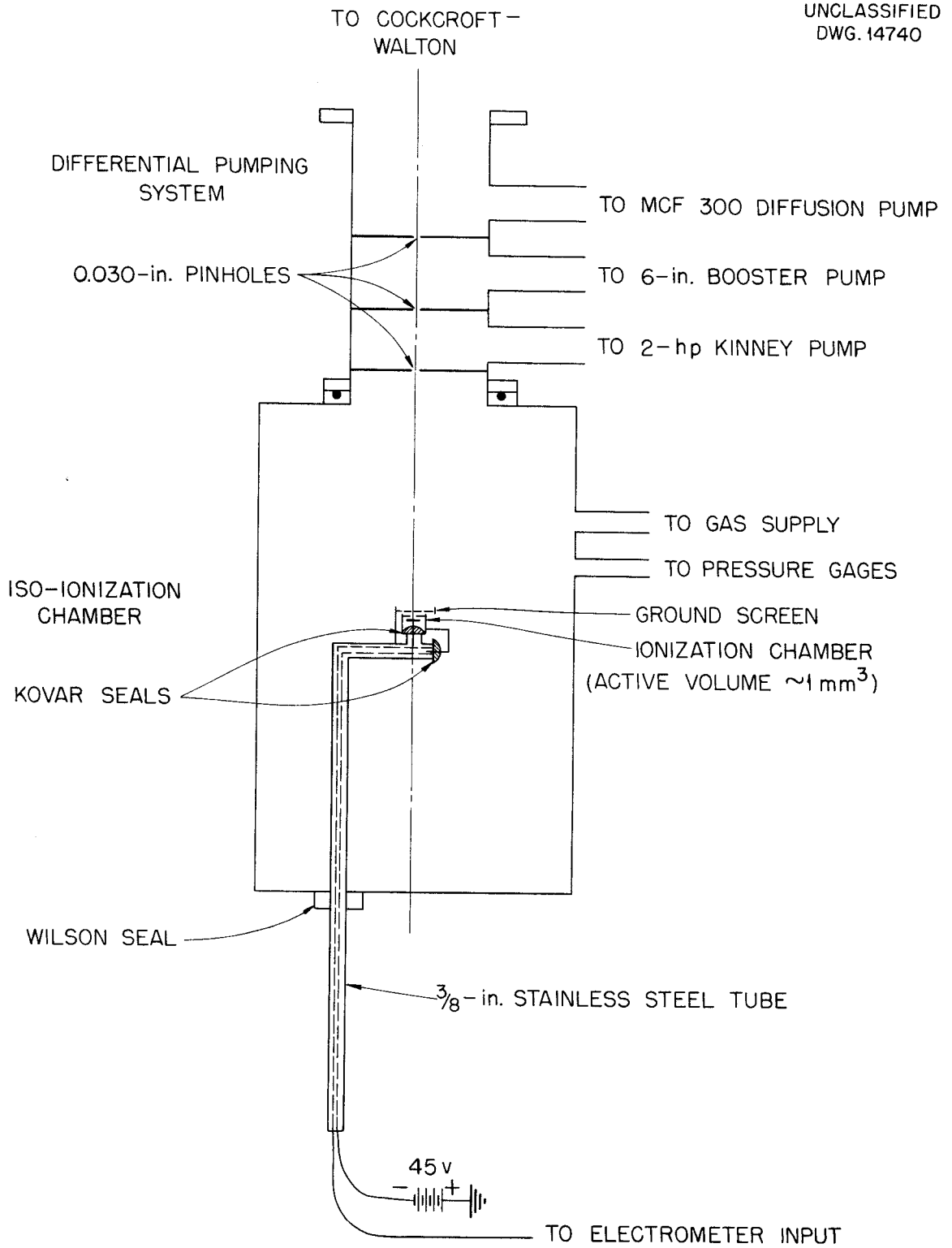


Fig. 5.1. Differential Pumping System and Isoionization Chamber.

PHYSICS DIVISION QUARTERLY PROGRESS REPORT

UNCLASSIFIED
DWG. 14741

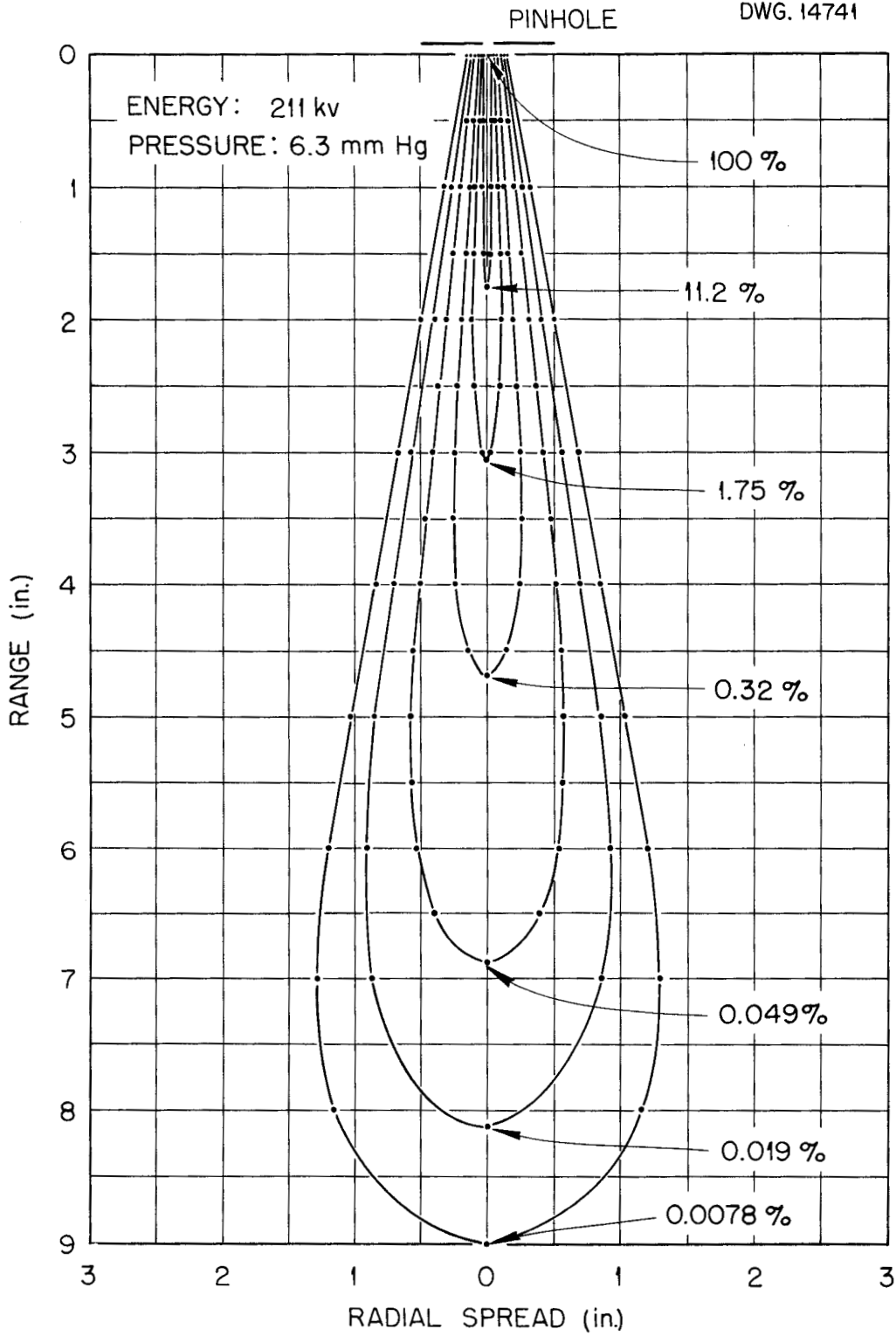


Fig. 5.2. Isoionization Density Contours for He^+ in Argon.

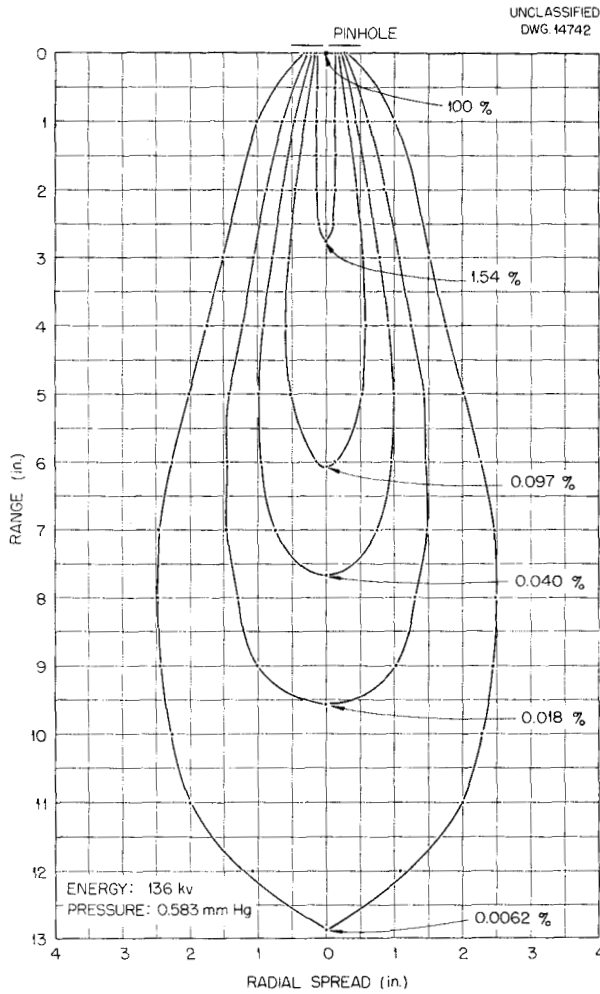


Fig. 5.3. Isoionization Density Contours for A^+ in Argon.

in a plane parallel to the axis of the beam for three typical incident ion-target gas combinations. The parameter, i , defining the contour shape is the ratio of ion chamber current at the point (R, r) to that at the point of entry of the ion beam into the gas target $(0, 0)$ expressed in per cent. The use of this relative rather than absolute ion chamber current corrects for minor fluctuations in beam current during the time of a given experiment.

It is noticeable in Figs. 5.2, 5.3, and 5.4 that the contours do not converge to a point at the origin of

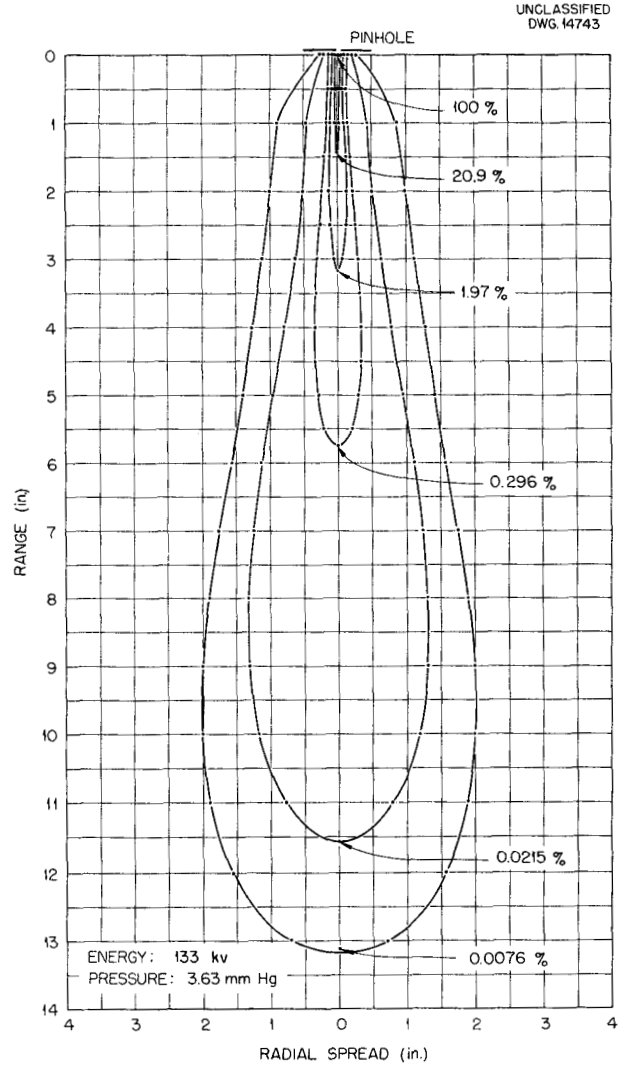


Fig. 5.4. Isoionization Density Contours for A^+ in Helium.

the beam at $(0, 0)$. A certain amount of experimental broadening of contours, for R very small, is to be expected from the finite sizes of the ion beam and the ion chamber. In addition to this effect, the contours for R very small are further spread in a lateral direction by scattering of the beam from the metal parts of the ion chamber itself, combined with reflection of scattered ions from the top plate of the target chamber. For very large values of r the contour

PHYSICS DIVISION QUARTERLY PROGRESS REPORT

shape may be distorted owing to reflection of ions from the side walls of the target chamber. Effects as a result of scattering from the walls of the system were minimized by determining ionization density distributions at a series of pressures. Since the size of a given contour increases as the pressure decreases, it was found possible to select appropriate pressures so as to give large enough values of R and r for accurate position measurement, yet small enough to avoid distortion near the walls.

An examination of Figs. 5.2, 5.3, and 5.4 shows that the contour shapes are quite different for the three cases. The A^+ in argon contours are quite broad as a result of the high probability of large angle scattering when the masses of incident and scattering particles are equal. The shapes for A^+ in helium and He^+ in argon are quite similar except that contours for A^+ in helium are broader for small values of R . This probably occurs because in small angle scattering (grazing collisions) the recoil He^+ ions in A^+ in helium are more effective in producing ionization than the recoil A^+ ions in He^+ in argon.

To compare results obtained at different pressures, it is necessary to know how the contour shape and size transform with pressure. If

$$R_B = \frac{25.4PR}{760} \text{ and } r_B = \frac{25.4Pr}{760},$$

then to a first approximation R_B and r_B represent lengths and widths, respectively, in millimeters at 1 atm corresponding to the values R and r in inches at pressure P . It has been found experimentally (Figs. 5.5 through 5.10) that if i/P^2 is plotted against R_B or R_B/r_B , the resulting curve is pressure independent over the range of pressures used in the experiments.

The ratio R_B/r_B is the ratio of the length of a given contour to its maximum half-width. Figure 5.11 shows isoionization density contours for He^+ in argon, A^+ in argon, and He^+ in helium as they would appear at the same pressure (1 atm). It should be noted that the abscissa and ordinate scales differ by a factor of 10.

If the values of i for $r = 0$ are plotted against the distance R , the resulting curve is seen to be nearly an exponential of the form $i = Ke^{-R}$, as shown in Fig. 5.12. The nature of the curve may be considered evidence that axial attenuation of the ionization is a result primarily of elastic scattering of incident particles out of the beam, which should be expected to yield an exponential decrease.

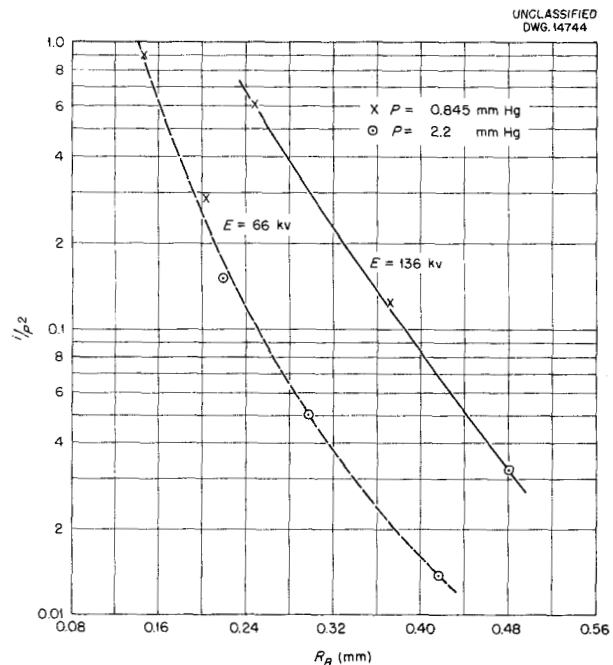


Fig. 5.5. Effect of Pressure on Contour Length of He^+ in Argon.

$$\left[\frac{\text{Contour per cent}}{(\text{Pressure})^2} \right] \text{ vs.}$$

[Contour axial end point at NTP] .

UNCLASSIFIED
DWG. 14745

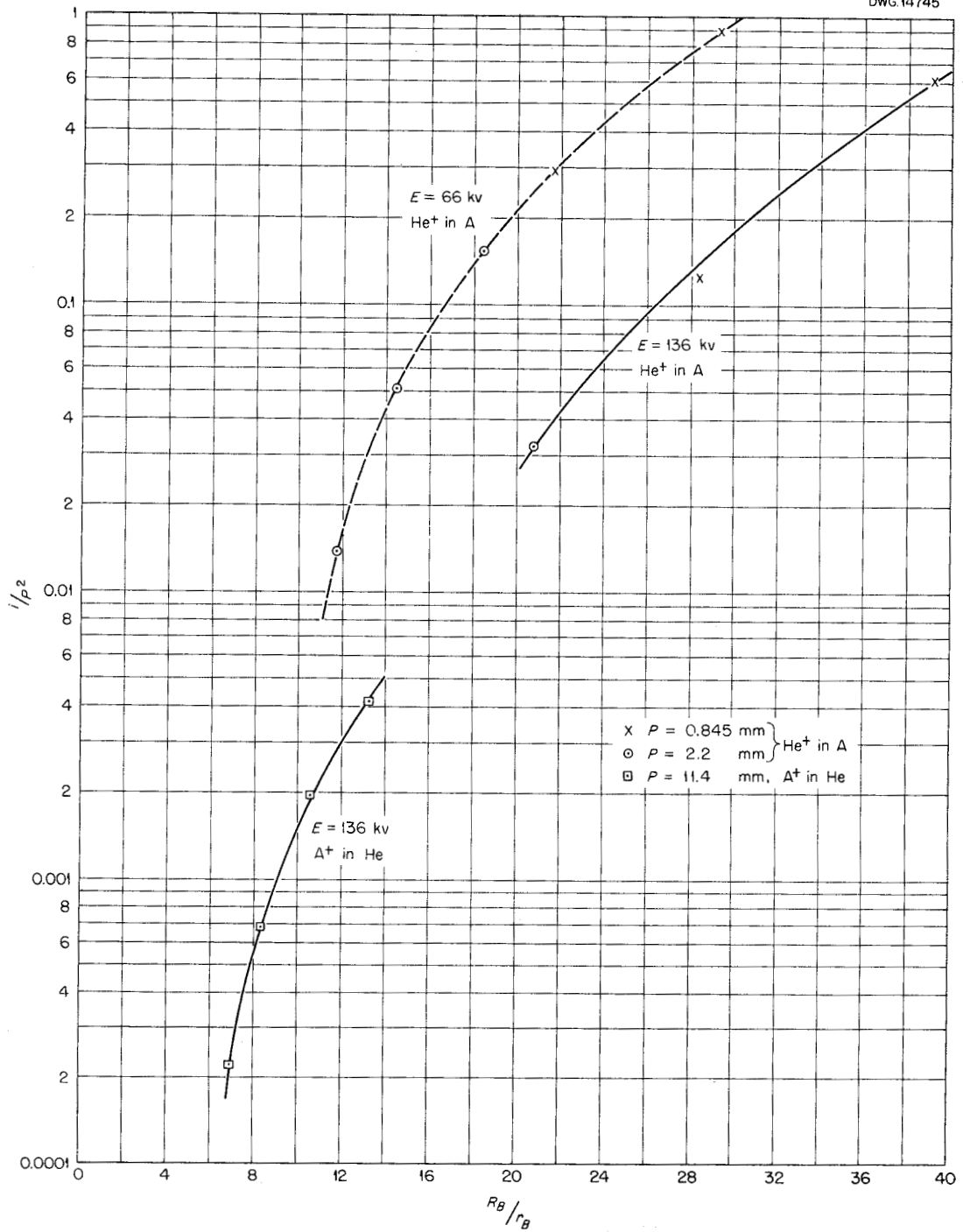


Fig. 5.6. Effect of Pressure on Contour Shape of He⁺ in Argon and A⁺ in Helium.

$$\left[\frac{\text{Contour per cent}}{(\text{Pressure})^2} \right] \text{ vs. } \left[\frac{\text{Contour axial end point}}{\text{Maximum contour half-width}} \right]$$

PHYSICS DIVISION QUARTERLY PROGRESS REPORT

If the values of i when R is a constant are plotted against r , the resulting curve is seen to be nearly a gaussian, as shown in Fig. 5.13. The solid curve fits the experimental data, whereas the dashed curve follows a gaussian fitted to the data at $r = 0$ and $r = 1$ inch.

Since the ionization density is known as a function of R and r , it should be possible to predict the response of an ionization chamber of arbitrary size by integrating the ionization density over the volume of

the chamber. For the geometry of a circular parallel plate chamber, this integral reduces to

$$i_c = A \int_0^a i(R_1, r) r dr ,$$

where i_c is the relative ion chamber current at saturation for a chamber of radius a placed at a distance R_1 from

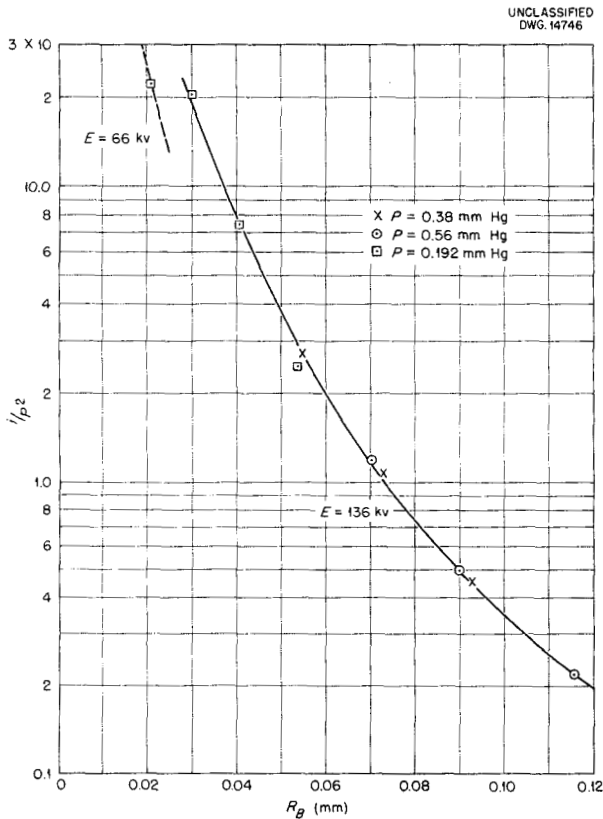


Fig. 5.7. Effect of Pressure on Contour Length of A^+ in Argon.

$$\left[\frac{\text{Contour per cent}}{(\text{Pressure})^2} \right] \text{ vs. } [\text{Contour axial end point at NTP}] .$$

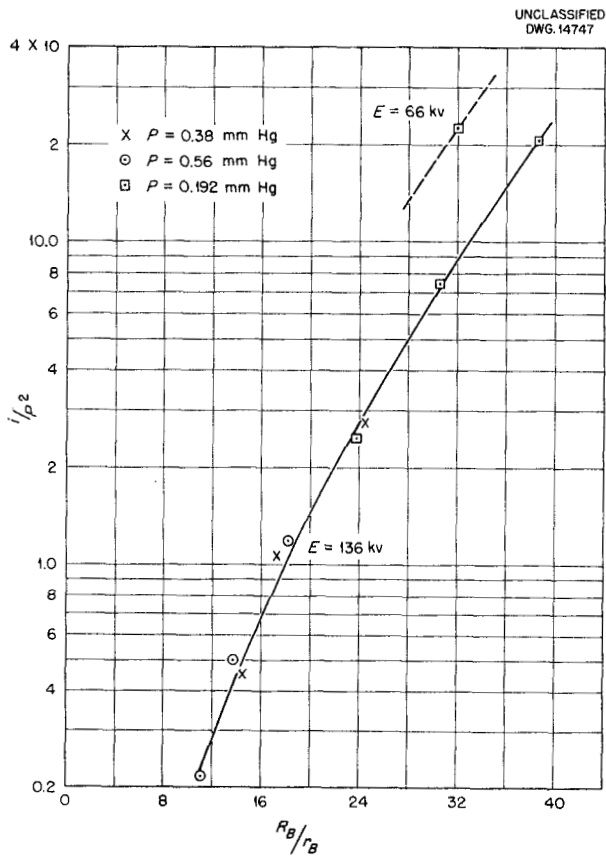


Fig. 5.8. Effect of Pressure on Contour Shape of A^+ in Argon.

$$\left[\frac{\text{Contour per cent}}{(\text{Pressure})^2} \right] \text{ vs. } \left[\frac{\text{Contour axial end point}}{\text{Maximum contour half-width}} \right] .$$

UNCLASSIFIED
DWG.14748

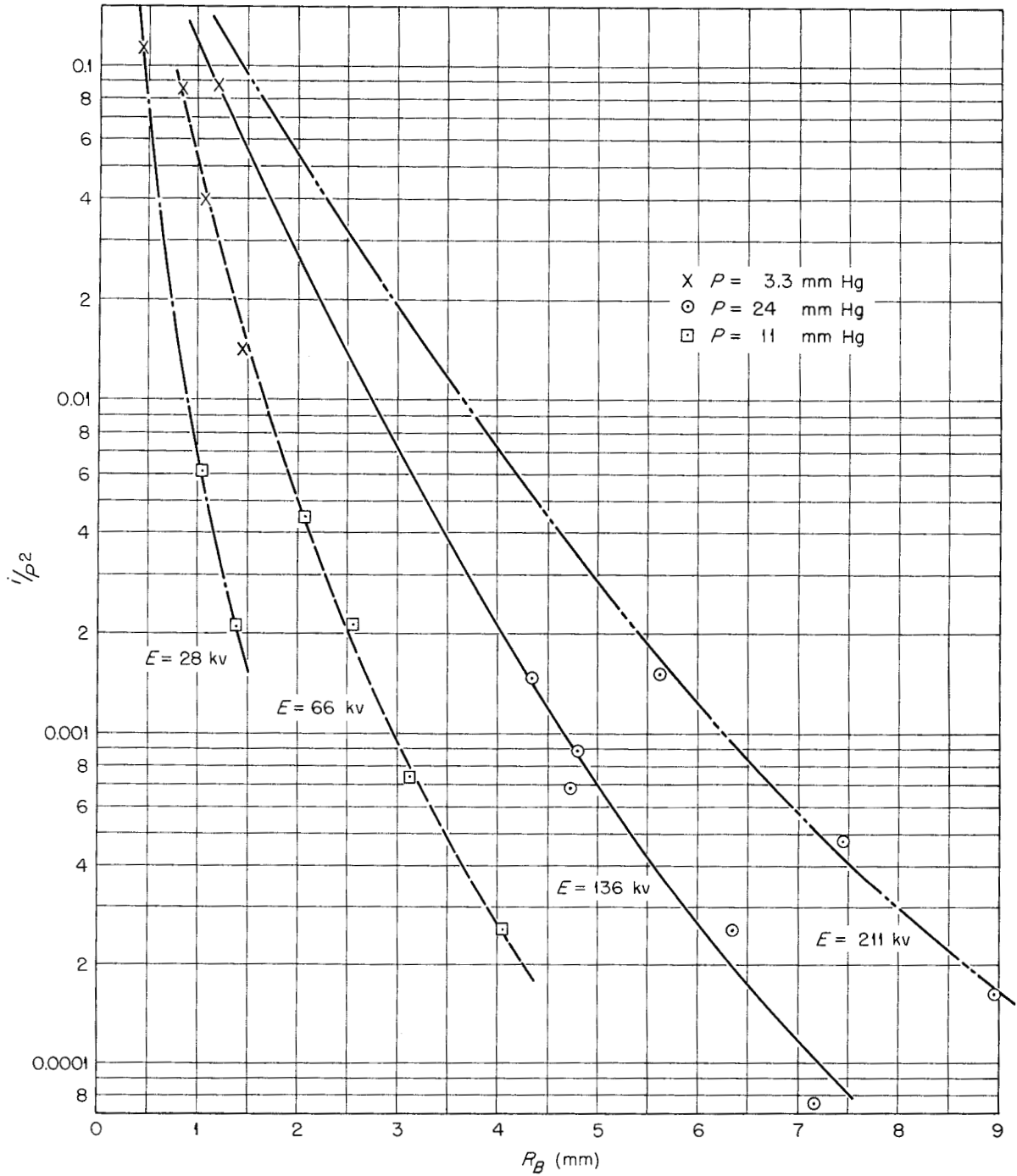


Fig. 5.9. Effect of Pressure on Contour Length of He^+ in Helium.

$$\left[\frac{\text{Contour per cent}}{(\text{Pressure})^2} \right] \text{ vs. } [\text{Contour axial end point at NTP}].$$

PHYSICS DIVISION QUARTERLY PROGRESS REPORT

UNCLASSIFIED
DWG. 14749

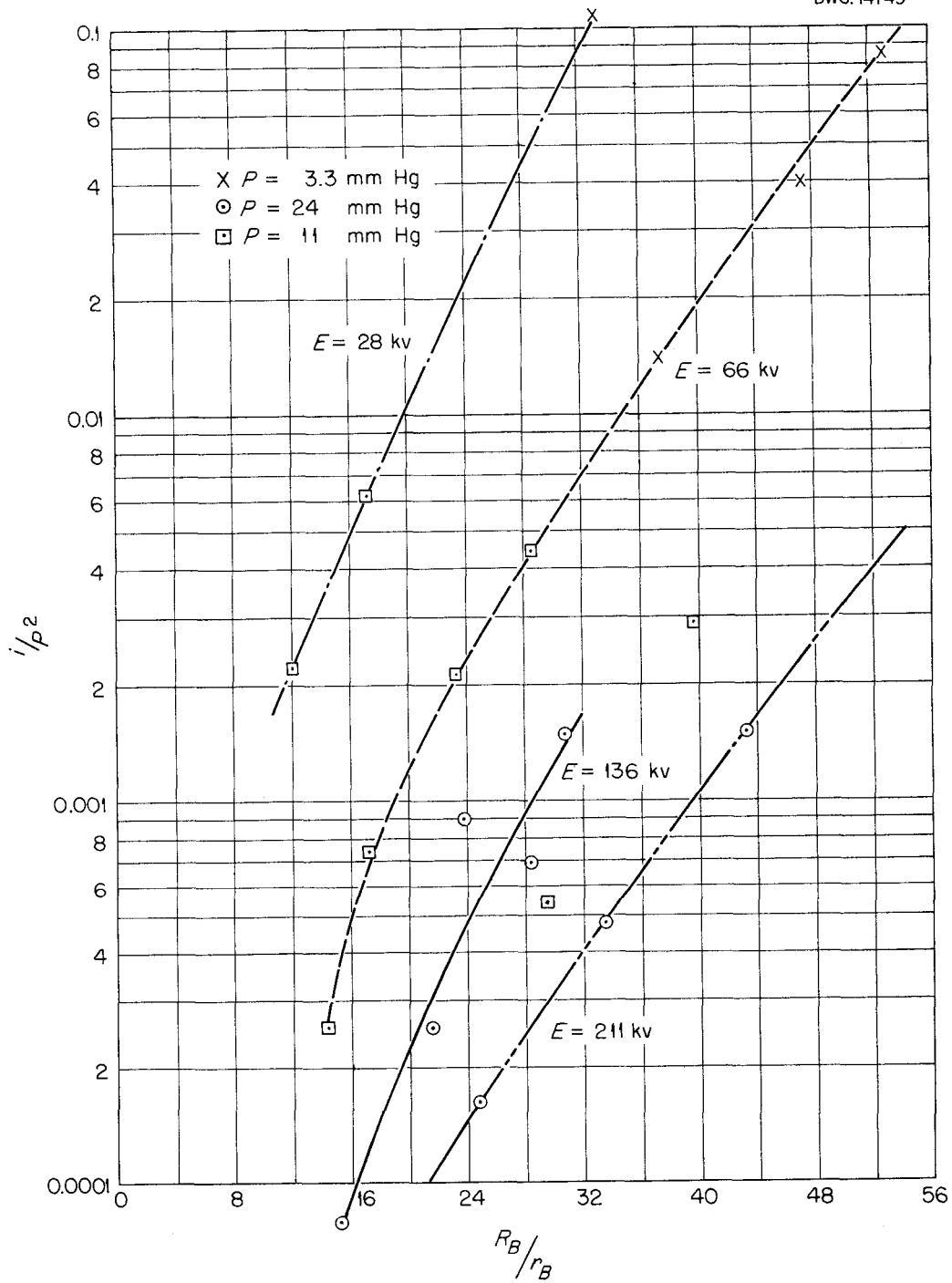


Fig. 5.10. Effect of Pressure on Contour Shape of He^+ in Helium.

$$\left[\frac{\text{Contour per cent}}{(\text{Pressure})^2} \right] \text{ vs. } \left[\frac{\text{Contour axial end point}}{\text{Maximum contour half-width}} \right]$$

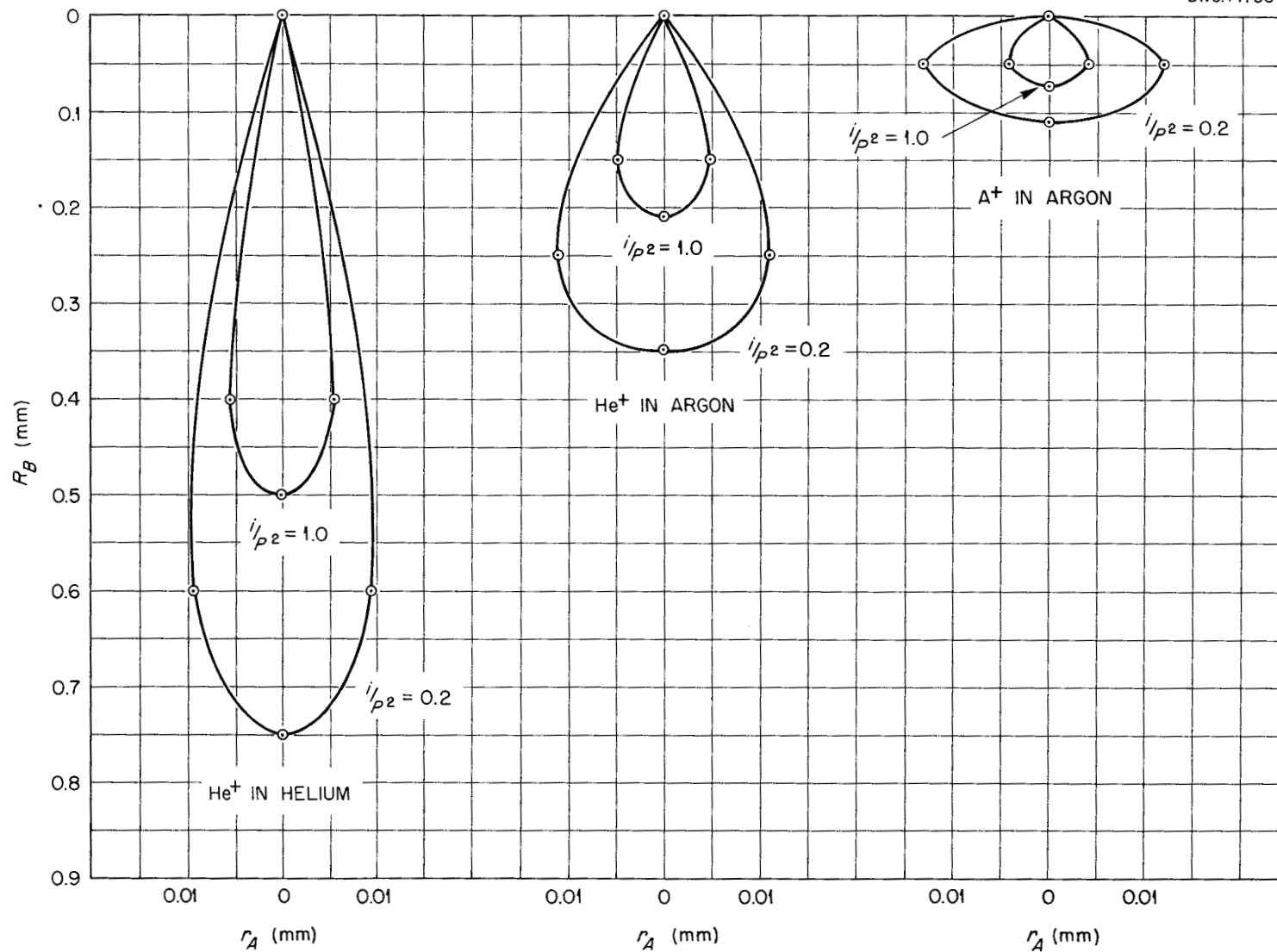


Fig. 5.11. Isoionization Density Contours of i/P^2 Equal to 1.0 and 0.2 for He^+ in Helium, He^+ in Argon, and A^+ in Argon, Each Converted to Atmospheric Pressure.

PHYSICS DIVISION QUARTERLY PROGRESS REPORT

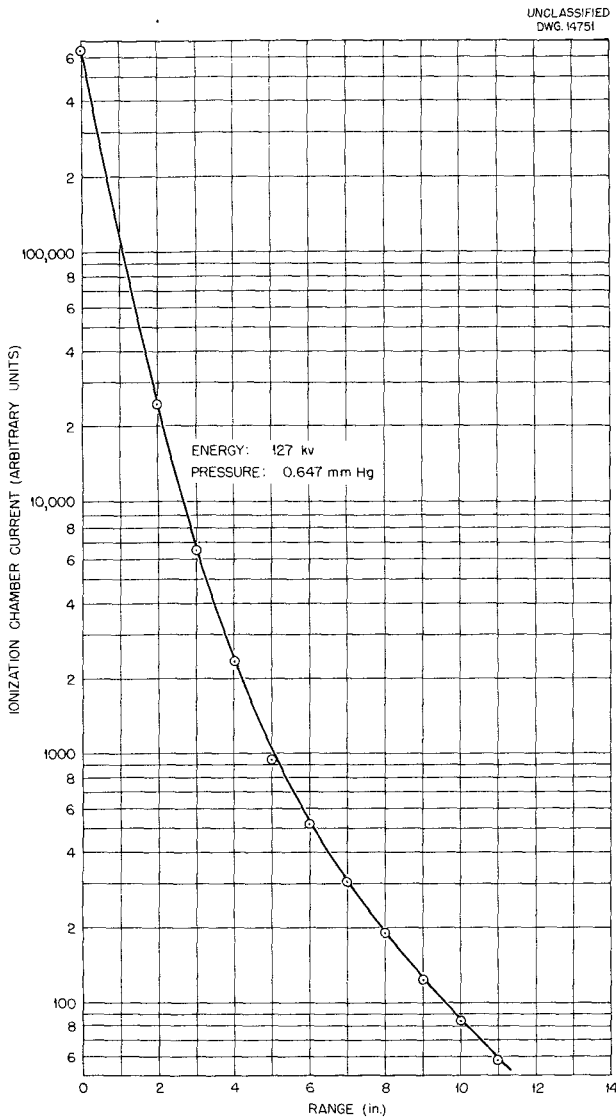


Fig. 5.12. Axial Ionization Chamber Current for A^+ in Argon.

the entrance pinhole. A typical plot of ir used for the graphical integration of $\int ir dr$ is shown in Fig. 5.14. The ionization chamber used in the determination of the extrapolated ionization range reported in the previous quarterly report was 3 in. in diameter, so that by computing

$$\int_0^{1.5} ir dr$$

for various values of R and plotting the results against R it was possible to check the previous data and the present assumptions. In Fig. 5.15 the solid curve is the plot of ion chamber response vs. distance as read with the 3-in. ion chamber, whereas the circled points are computed by integration of ionization density. To permit comparison of the experimental and computed curves, the computed curve is normalized to fit the experimental data at $R = 1$ inch. The agreement is quite good considering the difficulty of obtaining good graphical integrals, especially for R small.

The effect of pressure upon the measured value of the extrapolated ionization range was described in the previous quarterly report, and it was postulated that the observed effects were the result of elastic scattering of particles into values of r greater than the radius of the ion chamber. This postulate has been confirmed by the present study of the space distribution of ionization. Figure 5.14 shows that an appreciable portion of the ionization occurs for r greater than 1.5 in., and for larger values of R the maximum value of ir moves to still larger values of r . If

$$\int_0^{\infty} ir dr$$

is computed for various values of R and is plotted against R , as shown in Fig. 5.15, the straight line portion of this curve should extrapolate to the same value (R_E) defined in the previous quarterly report. The agreement is rather crude since a large percentage of the total ionization occurs for r greater than that which can be measured with the present equipment but is considered sufficiently good to serve as an additional verification of the postulated explanation of the pressure dependence of extrapolated ionization range.

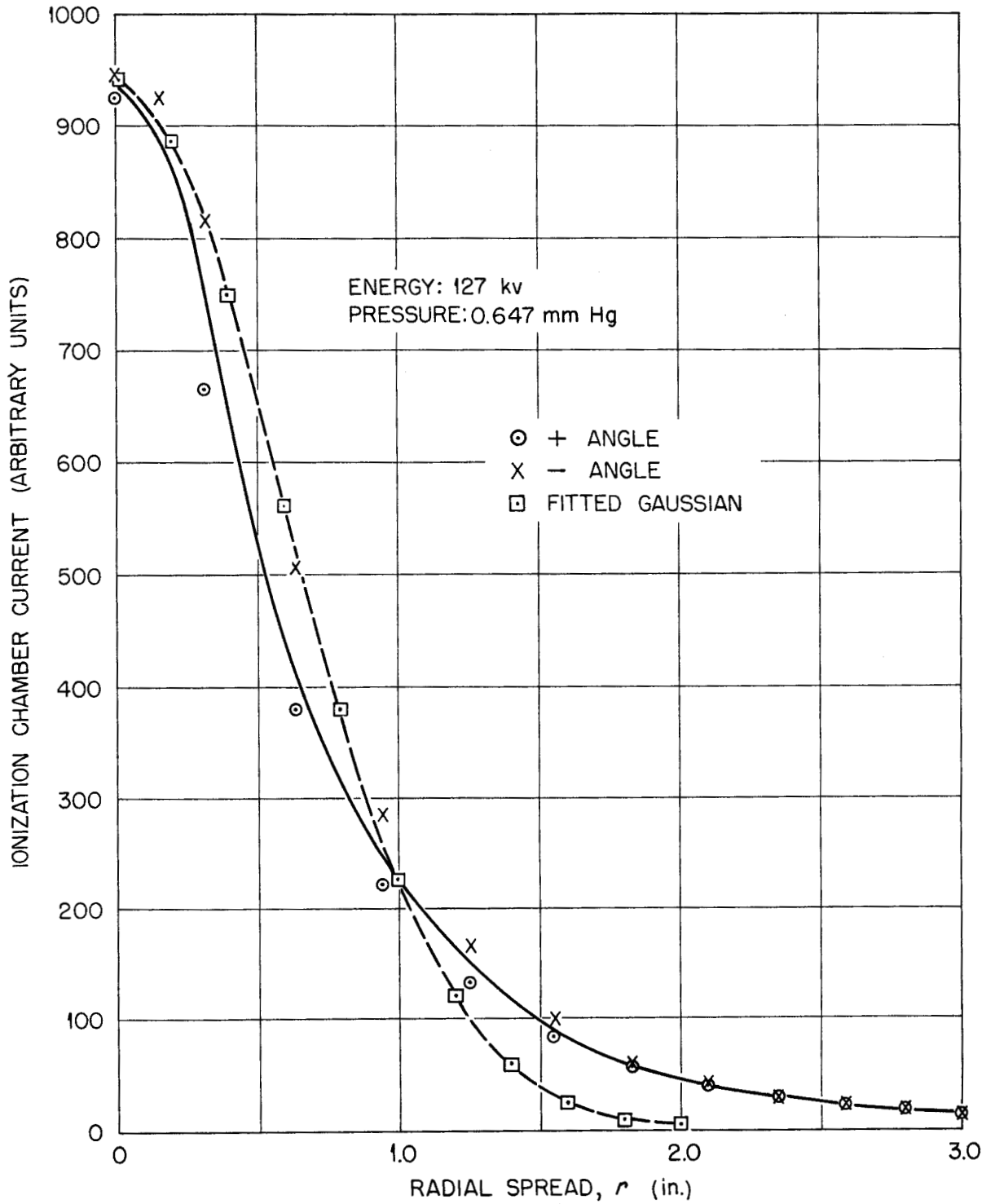


Fig. 5.13. Equirange Contour for $R = 5.0$ in., A^+ in Argon. Gaussian curve superimposed (dashed curve), matched at $r = 0$ in. and $r = 1$ inch.

PHYSICS DIVISION QUARTERLY PROGRESS REPORT

UNCLASSIFIED
DWG. 14753

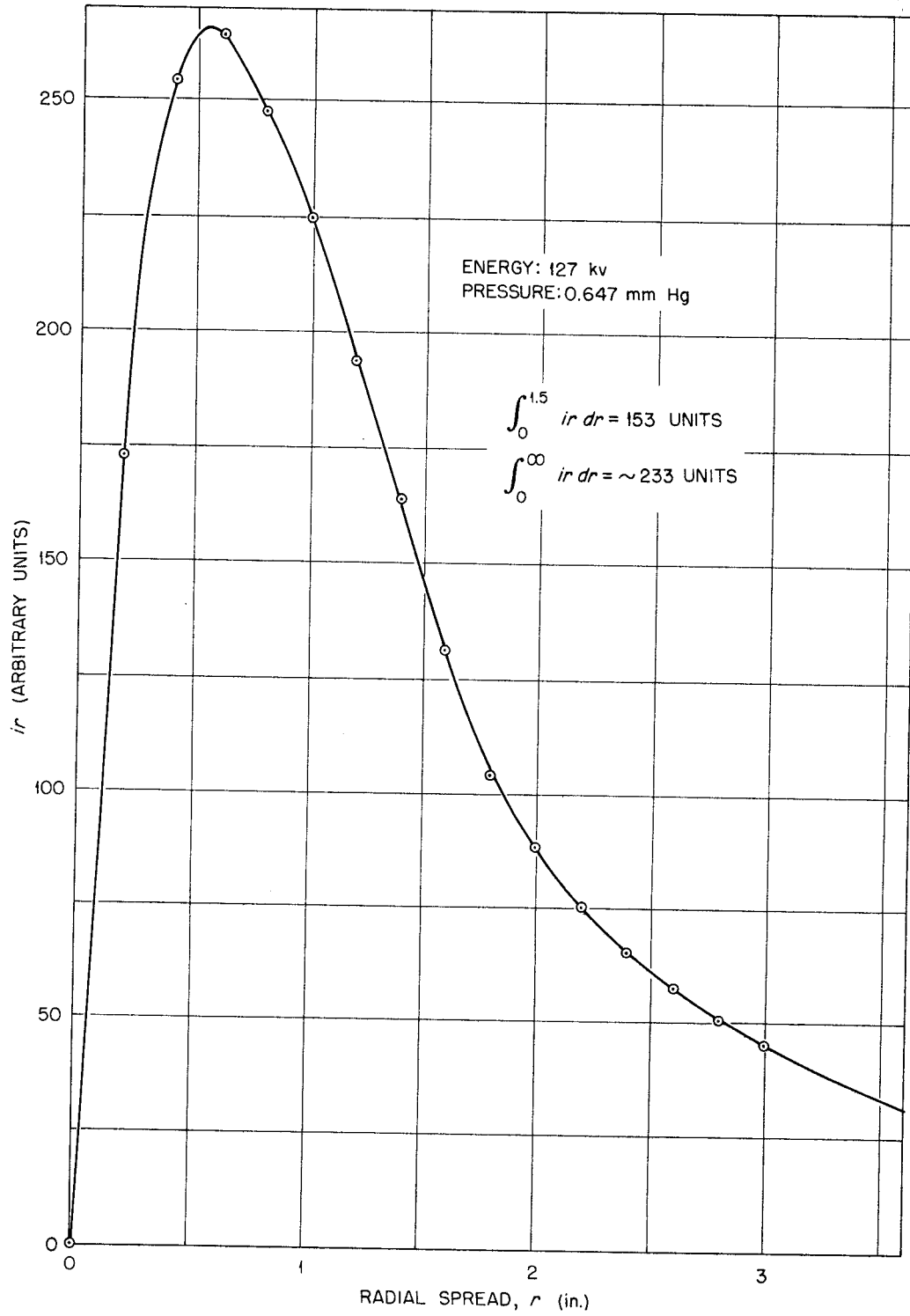


Fig. 5.14. Integration of $ir dr$ for A^+ in Argon for $R = 5.0$ inches.

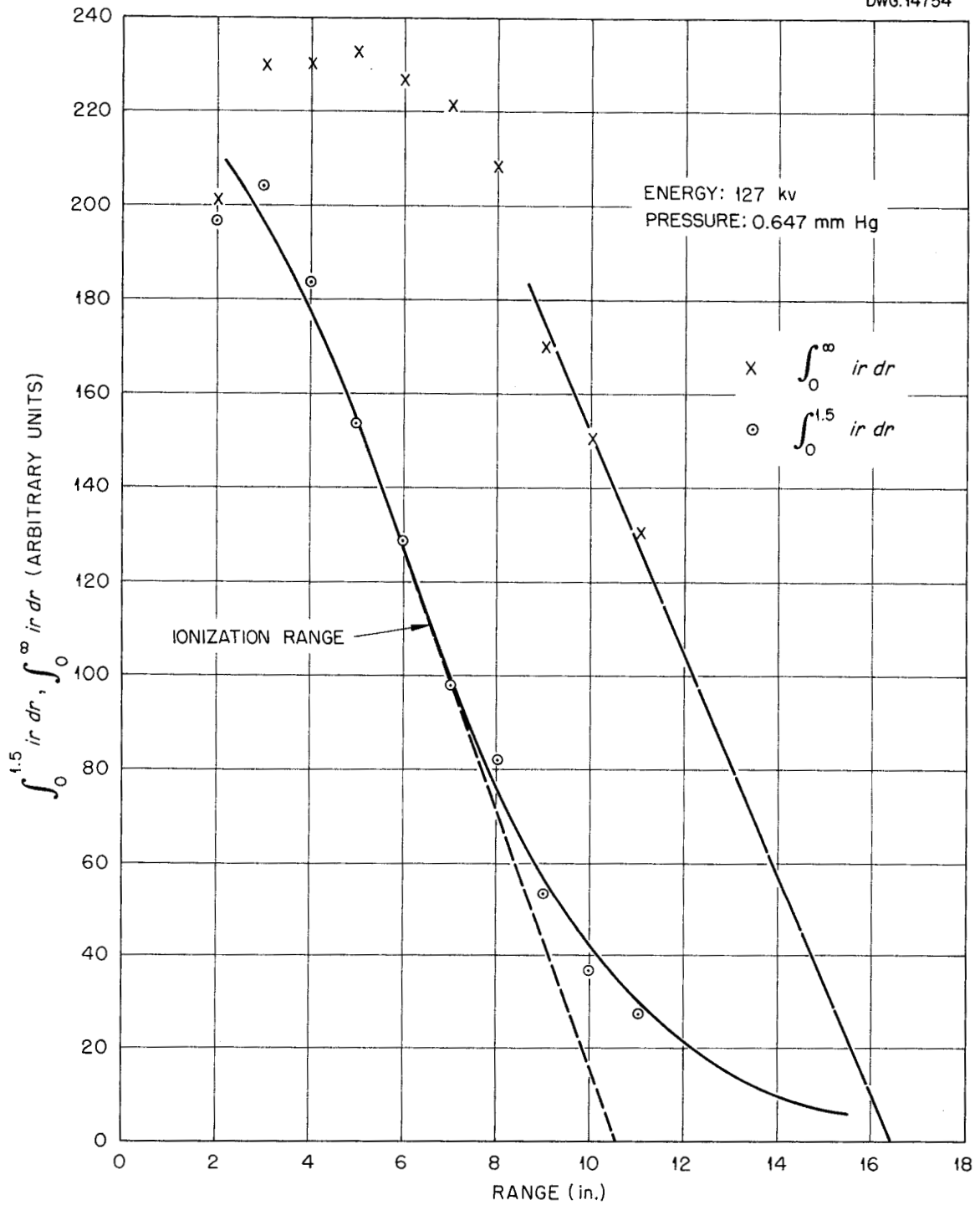


Fig. 5.15. Computation of Range from Isoionization Data. $\int_0^{1.5} ir dr$ and $\int_0^{\infty} ir dr$ as a function of range compared with ionization range curve (solid line) measured with 3-in. ionization chamber for A^+ in argon.

PHYSICS DIVISION QUARTERLY PROGRESS REPORT

Workers at the University of Nebraska⁽²⁾ have observed similar pressure effects under somewhat different experimental conditions. It has been found in the present research that the entire "pressure effect" can be explained in terms of the elastic scattering and finite chamber size, without recourse to postulates of accumulative ionization. Accumulative ionization, if it occurs under the experimental conditions at this laboratory, must be considered to be a minor effect.

The family of isoionization density contours (curves of constant i at varying R and r) may be expressed by an empirical formula of the form

$$i = e^{-AR - Br^2/R^2} .$$

A contour produced by A^+ in argon is plotted in Fig. 5.16 along with computed values of i from the formula.

(2) C. J. Cook, E. Jones, and T. Jorgensen, *Range of Protons in Hydrogen and Oxygen*, AECU-1890.

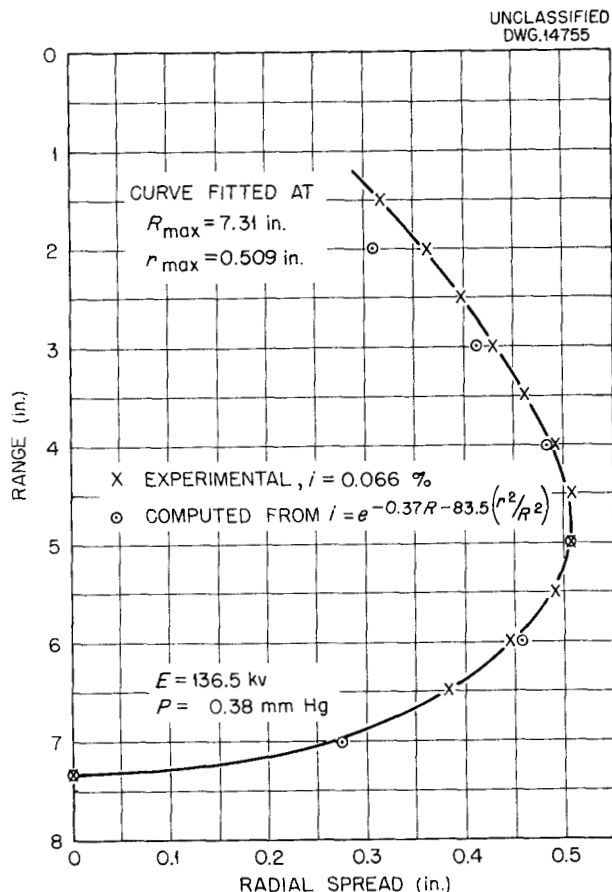


Fig. 5.16. Curve Fitting of the Function $i(R, r) = e^{-AR - B(r^2/R^2)}$ for A^+ in Argon.

6. NEUTRON DECAY AND NEUTRON CROSS SECTIONS

NEUTRON DECAY

F. Pleasonton H. L. Reynolds
 A. H. Snell

Difficulties have been experienced in the absolute determination of the neutron half life. For efficient counting of the coincidences between beta particles and recoil protons, the beta counter (now a thin anthracene crystal) should be placed near the portion of the neutron beam that serves as the source. This places the beta counter only a few inches from

the proton counter and raises the possibility of genuine but undesired coincidences arising from particles in the background radiation that travel rapidly between the two detectors. Previously these coincidences had not been considered because advantage was taken of the finite collecting time (0.1 to 1 μ sec) of the protons. Separation could then be obtained by proper use of delay lines. It now appears that with the present electronic circuits this technique is not quite good enough for the absolutely clean separation required. The circuit

revision required is fairly drastic but will be useful for the angular distribution experiment described here.

With the presence of intense beams from the LITR, the possibility also arises of improving the proton collection by using a beam of much smaller diameter. With these considerations in mind, the half-life determination is being accented less at present than is the consideration of the more exciting problem of the beta-proton angular correlation.

The possible angular distribution for beta decay using invariant interaction can be expressed as $(1 + n\beta\cos\theta)$, where β is the electron velocity in terms of the velocity of light, θ is the angle between the electron and the neutrino, and n is a number between 1 and -1 that depends upon the coupling between the electron-neutrino field and the nucleons. The value of n can be determined in several ways. Two methods of attack are planned, and the equipment is designed to be adaptable to either.

The first method involves a measurement of the momentum spectrum of the recoil proton. The spectrum is quite sensitive to the value of n . The theoretical ratios of the number of recoils occurring with momentum (P) in rest mass units between 1.8 and 2.2 to the number between 1.2 and 1.6 for various values of n are as follows:

n	RATIO
1	2.08
1/3	1.47
-1/3	0.98
-1	0.61

A thin magnetic lens and regulated current supply is now operating satisfactorily with a transmission of

approximately 6% and a momentum resolution of 20%. It is estimated that the counting rate for recoil protons will be roughly 10 per minute with this lens. The major difficulty will be to reduce the background counting rate to this value. Elaborate shielding is envisioned, and a major effort has been made to design an electrostatic focusing system for the proton after the lens, so that a small electron multiplier proton counter may be used. The first multiplier plate has an area of 1 square inch. The proton has a maximum energy of 750 ev. Therefore a pressure of less than 10^{-6} mm of mercury must be maintained in the spectrometer to avoid interaction of the protons with gas molecules.

The angular distribution of the electron relative to the direction of the recoil proton depends upon the value of n . The theoretical ratios of the number of events with angles between 125 and 145 deg to those between 170 and 190 deg for various values of n are as follows:

n	RATIO
1	0.128
1/3	0.098
-1/3	0.077
-1	0.064

A symmetrical arrangement of two proton counting multipliers and two scintillation counters to observe simultaneously the angles 135 deg and 180 ± 10 deg is under construction. A coincidence circuit has been designed to take advantage of the transit time of the protons to eliminate true coincidences that result from causes other than the neutron decay. The estimated coincidence counting rate is approximately 0.2 count/min with a background equal to or slightly less than this number. The evaluation of the relative transmission of the collimating systems has been started.

PHYSICS DIVISION QUARTERLY PROGRESS REPORT

All equipment including the neutron collimator and beam stopper will be in operation on June 1.

TIME-OF-FLIGHT SPECTROMETER

G. S. Pawlicki E. C. Smith

The neutron time-of-flight spectrometer has been operated at a resolution somewhat better than $1.2 \mu\text{sec}/\text{meter}$. The results of preliminary measurements of indium isotopes are shown in Fig. 6.1. The upper curve is the transmission of $4.273 \text{ g}/\text{cm}^2$ of natural indium oxide, which has two isotopes with the relative abundances of 95.8% In^{115} and 4.2% In^{113} . The middle curve is the transmission of $4.3 \text{ g}/\text{cm}^2$ of In_2O_3 depleted to 0.2% in the In^{113} isotope. The bottom curve is the transmission of $0.86 \text{ g}/\text{cm}^2$ of In_2O_3 with the isotopic composition 77.2% In^{115} , 22.8% In^{113} . It is to be noted that the enriched samples had approximately the same number of grams per square centimeter of one isotope as the natural sample, but were depleted in the other isotope. The energies of the resonances observed above 6 eV are as follows:

In^{113}	In^{115}
$14.3 \pm 0.5 \text{ eV}$	$8.86 \pm 0.22 \text{ eV}$
21	12
25	22
31	40
40 (several unresolved levels)	93 (several unresolved levels)
93 (?)	
2200	

A preliminary investigation of copper reveals levels at $700 \pm 100 \text{ eV}$ and $2200 \pm 600 \text{ eV}$.

PILE OSCILLATOR MEASUREMENTS

H. Pomerance T. Arnette

The thermal-neutron capture cross sections of several separated stable isotopes obtained from Y-12 have been measured (see Table 6.1). The standard against which they are compared is 95 barns for gold. The atomic cross section (or natural element cross section) is the sum of the isotopic values multiplied by the corresponding natural abundances.

Five service measurements were made for the G-E project. A summary report of all measurements made of separated isotopes is being prepared.

TABLE 6.1

Capture Cross Sections

ISOTOPE	ISOTOPIC CROSS SECTION (barns)	ESTIMATED ERROR (%)	ATOMIC CROSS SECTION (barns)
K^{40}	75	Tentative	0.01
Ca^{40}	0.22	(20)*	0.21
Ca^{42}	40	8	0.25
Fe^{54}	2.18	8	0.13
Fe^{56}	2.55	8	2.34
Fe^{57}	2.36	12	0.05
Fe^{58}	2.5	80	0.02
Ba^{134}	2	100	0.06
Ba^{135}	5.6	15	0.37
Ba^{136}	0.4	100	0.03
Ba^{137}	4.9	8	0.55
Ba^{138}	0.68	15	0.49

* The Ca^{43} contribution is unknown.

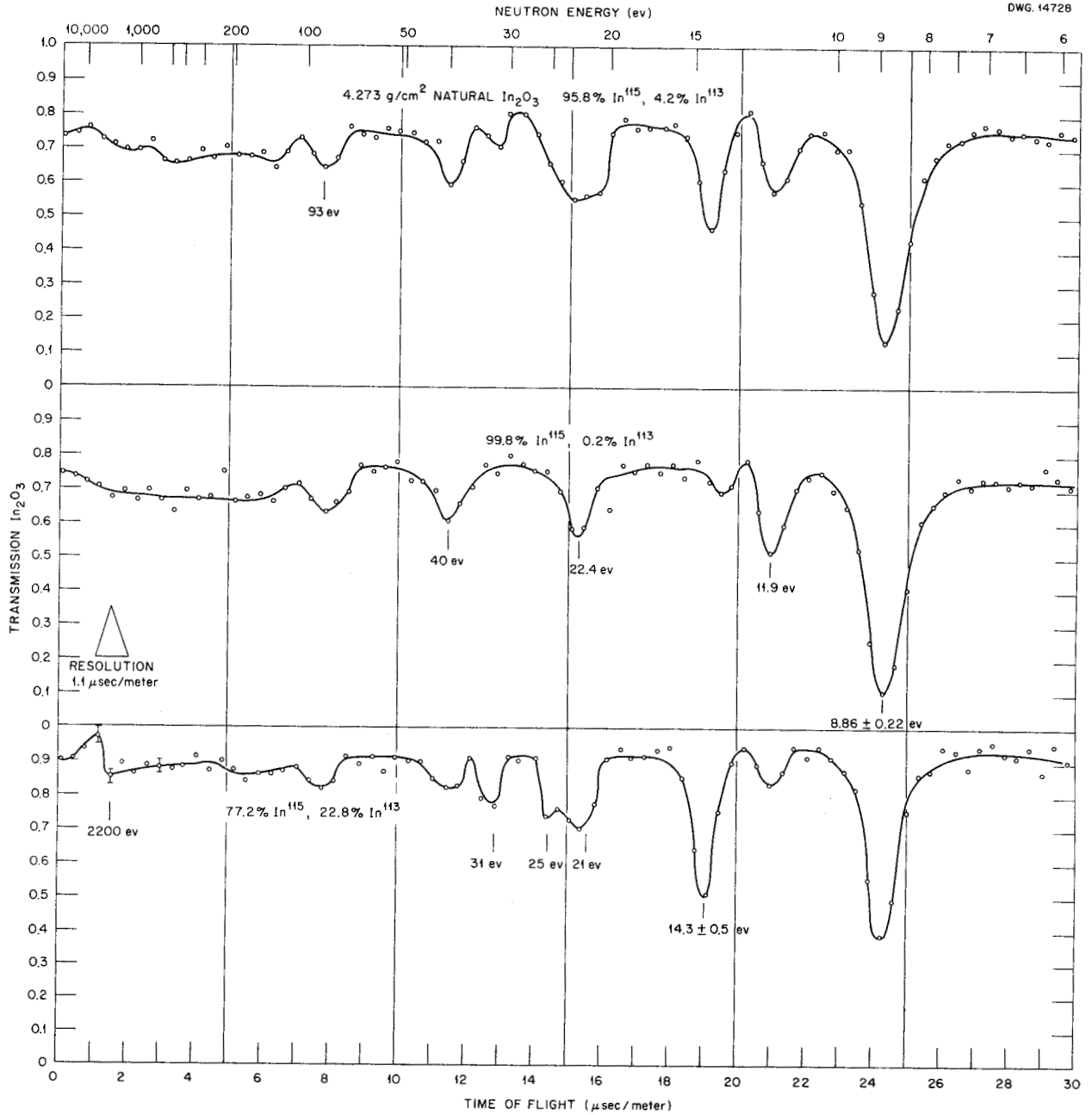


Fig. 6.1. Transmission Measurements of Indium Isotopes with Time-of-Flight Spectrometer.

PHYSICS DIVISION QUARTERLY PROGRESS REPORT

7. THEORETICAL PHYSICS

STATUS OF CURRENT WORK

M. E. Rose

Activities during this quarter have been confined to the continuation of projects already well begun and described in previous reports. They are:

1. L-shell internal conversion coefficients - these are being computed on the SEAC in Washington and the screened potential field computations are now finished. Coding for the wave equation solutions is in progress.

2. Fermi functions for forbidden beta decay - the plan at present is that this work will be done on the Whirlwind computer at MIT.

3. Angular correlation of nuclear radiations (with L. C. Biedenharn) - numerical results for conversion correlation coefficients for transitions in which the conversion is mixed are now complete. Racah function tabulations needed for correlation work are now complete.

A series of lectures on beta decay has been started. The general purpose of these lectures is to examine as carefully as possible the directions in which future work in beta decay ought to go. The need for a more complete analysis of some published results on beta decay has become evident, and it is expected that the work on the Fermi functions (item 2) will be helpful.

TABULATION OF THE RACAH COEFFICIENTS

L. C. Biedenharn

The tabulation of the Racah coefficients performed by the Mathematics

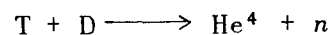
Panel has been completed and a laboratory report has been issued.⁽¹⁾ The material contained in this report has been extended and submitted to the *Reviews of Modern Physics* for publication as a paper entitled "Tables of the Racah and Associated Coefficients" in joint authorship with J. M. Blatt, University of Illinois, and M. E. Rose of this Laboratory.

A paper entitled "An Identity Satisfied by the Racah Coefficients" by L. C. Biedenharn has been accepted for publication by the *Journal of Mathematics and Physics* (MIT).

THEORY OF THE T + D REACTION

A. Simon

In a recent paper⁽²⁾ Flowers has fitted the experimental points for the reaction



by postulating a single common resonance, at some negative energy, for the two principal entrance channels ${}^2S \longrightarrow {}^2S$ and ${}^4S \longrightarrow {}^2D_{3/2}$. This reaction cross section can be completely expressed in terms of the logarithmic derivative of the incident particle's wave function evaluated at the nuclear surface.⁽³⁾ To obtain this quantity Flowers used a single particle model in which the bombarding triton moves in a square well of depth W_0 (≈ 22.2 Mev) and range c ($= 6.95 \times$

(1) L. C. Biedenharn, *Tables of the Racah Coefficients*, ORNL-1098 (April 8, 1952).

(2) B. H. Flowers, "The Theory of the T + D Reaction," *Proc. Roy. Soc. (London)* **A204**, 503 (1951).

(3) H. Feshbach, D. C. Peaslee, and V. F. Weisskopf, "On the Scattering and Absorption of Particles by Atomic Nuclei," *Phys. Rev.* **71**, 145 (1947).

10^{-13} cm). The resulting logarithmic derivative is observed to be

$$\left[\frac{\phi}{\phi'} \right]_{r=c} = \frac{\tan \bar{K}C}{\bar{K}}$$

where

$$\bar{K} = \sqrt{\frac{2M}{\hbar^2} \left[E + W_0 + \frac{i\Gamma}{2} \right]}$$

and the imaginary term represents the effect of absorption. The center of mass energy is denoted by E .

If it is then assumed that $\Gamma/W_0 \ll 1$, as is necessary for the occurrence of resonances, it can be observed that

$$\left[\frac{\phi}{\phi'} \right]_{r=c} \approx \frac{\tan Kc}{K \left[1 + \frac{\Gamma^2(Kc)^2}{16(E + W_0)^2} \tan^2 Kc \right]} + \frac{i\Gamma c \sec^2 Kc}{4(E + W_0) \left[1 + \frac{\Gamma^2(Kc)^2}{16(E + W_0)^2} \tan^2 Kc \right]}$$

where

$$K = \frac{2M}{\sqrt{\hbar^2}} (E + W_0)$$

The term in $(\Gamma/W_0)^2$ is neglected by Flowers. However, it is clear that this term cannot be omitted near a resonance since $\tan Kc = \infty$ at such a point. Equation (13) in Flowers' work⁽²⁾ leads to a reaction cross section that is zero at resonance.

The corrections to the logarithmic derivative have been computed at several energies by using the parameters mentioned in the previous reference.⁽²⁾ The real and the imaginary parts must be multiplied by the correction factor that follows:

E_{kev}	0	120	240
ϵ	0.644	0.791	0.850

The revised cross section has also been computed by using the same parameters (Γ and W_0).⁽²⁾ The new curve no longer fits the experimental data. An attempt is being made to fit the experimental points by using the one-level formula with exact coulomb wave functions.

THE PARAMETERIZATION OF QUANTUM ELECTRODYNAMICS

T. A. Welton

The single-particle formulation of relativistic quantum electrodynamics, given in the preceding quarterly report,⁽⁴⁾ has been extended in several directions. The one-particle theory can be conveniently regarded as one that follows from the introduction of a fifth parameter (in addition to the space and time coordinates) into the usual theory. This parameter is, classically, the proper time, which can be used to put the relativistic equations in a form symmetrical in the four space-time coordinates. With some obvious changes of notation from the previous report, the wave equation becomes

$$i\dot{\psi} = M\psi, \quad (1)$$

(4) T. A. Welton, "A Rational One-Particle Relativistic Electron Theory," *Physics Division Quarterly Progress Report for Period Ending December 20, 1951*, ORNL-1278, p. 25.

PHYSICS DIVISION QUARTERLY PROGRESS REPORT

where M is the mass operator, identical with the operator K previously defined. The dot indicates differentiation with respect to the proper time variable, s .

With this change, cross sections can be calculated for one-electron processes (elastic scattering, Compton effect, bremsstrahlung, and radiative corrections to these cross sections) in addition to the mass correction shown previously. Pair annihilation (but not production) can be calculated by taking the transition rate per unit proper time from a state with positive dt/ds to one with negative dt/ds .

A very similar formalism has been devised for the description of spin zero particles by using for the free particle mass operator,

$$M = i\beta^\mu \frac{\partial}{\partial x^\mu}, \quad (2)$$

where the β^μ are the four five-by-five matrices introduced by Kemmer. In the usual formalism the spin zero and spin one-half formalisms are not at all parallel, and the self-energies are widely different. In the present theory, the calculations are exactly parallel; the self-energies both diverge logarithmically and the only differences are detailed differences obviously related to the interaction of the spin with the light waves.

An interesting result is that a rationale appears for the mass renormalization. The divergence of the mass correction is associated with a similar divergence of the norm of the first-order corrected wave function. In other words, the perturbation theory is invalid for the calculation of the very high-frequency contributions to the mass perturbation. Presumably, then, no real divergence occurs, and the renormalization is a perfectly believable recipe.

A further extension has been made to allow the possibility of pair production. This is done by a formal analogue of the usual second quantization. The wave function is treated as an operator and a wave functional (Ψ) of ψ is introduced. The wave equation is

$$i\dot{\Psi} = [\int dx (\bar{\psi} M \psi)] \Psi, \quad (3)$$

where ψ and $\bar{\psi}$ satisfy anticommutation relations,

$$\begin{aligned} & [\psi_i(x, s), \psi_j(x', s)]_+ \\ &= [\bar{\psi}_i(x, s), \bar{\psi}_j(x', s)]_+ = 0, \end{aligned}$$

$$\begin{aligned} & [\psi_i(x, s), \bar{\psi}_j(x', s)]_+ \\ &= \delta_{ij} \delta(x - x'). \end{aligned} \quad (4)$$

These hold for the spin one-half case, where

$$\bar{\psi} = \psi^\dagger \gamma^0 \quad (5)$$

and i and j refer to the four-valued spin variable. Presumably, commutation rules must be assumed for the spin zero case, and the relation between $\bar{\psi}$ and ψ^\dagger is easily found.

The formalism based on Eqs. 3 and 4 has been used to calculate pair production and vacuum polarization. The results can be made to agree with the usual divergent ones, but this is not necessary and it is apparently possible to obtain pair production without any diverging vacuum polarization. This

FOR PERIOD ENDING MARCH 20, 1952

matter is under investigation, as is the question of the feasibility of a thorough calculation of the Lamb shift. Such a calculation seems quite

difficult, but could give unambiguous information as to the proper construction of the theory specified by Eqs. 3 and 4.